

UNCLASSIFIED

AD NUMBER

AD465722

LIMITATION CHANGES

TO:

Approved for public release; distribution is unlimited.

FROM:

Distribution authorized to U.S. Gov't. agencies and their contractors;
Administrative/Operational Use; APR 1965. Other requests shall be referred to Air Force Flight Dynamics Laboratory, FDFR, Wright-Patterson AFB, OH 45433.

AUTHORITY

affdl ltr, 21 dec 1974

THIS PAGE IS UNCLASSIFIED

FDL-TDR-64-153

CATALOGED BY: DDC
AS AD NO. 465722

EXPERIMENTAL DETERMINATION OF THE APPARENT MOMENT OF INERTIA OF PARACHUTES

TECHNICAL DOCUMENTARY REPORT No. FDL-TDR-64-153

APRIL 1965

AF FLIGHT DYNAMICS LABORATORY
RESEARCH AND TECHNOLOGY DIVISION
AIR FORCE SYSTEMS COMMAND
WRIGHT-PATTERSON AIR FORCE BASE, OHIO

Project No. 6065, Task No. 606503

(Prepared under Contract No. AF 33(657)-11184 by the
Department of Aeronautics and Engineering Mechanics,
University of Minnesota, Minneapolis, Minnesota;
Shukry K. Ibrahim, Author)

NOTICE: When government or other drawings, specifications or other data are used for any purpose other than in connection with a definitely related government procurement operation, the U. S. Government thereby incurs no responsibility, nor any obligation whatsoever; and the fact that the Government may have formulated, furnished, or in any way supplied the said drawings, specifications, or other data is not to be regarded by implication or otherwise as in any manner licensing the holder or any other person or corporation, or conveying any rights or permission to manufacture, use or sell any patented invention that may in any way be related thereto.

NOTICES

When Government drawings, specifications, or other data are used for any purpose other than in connection with a definitely related Government procurement operation, the United States Government thereby incurs no responsibility nor any obligation whatsoever; and the fact that the Government may have formulated, furnished, or in any way supplied the said drawings, specifications, or other data, is not to be regarded by implication or otherwise as in any manner licensing the holder or any other person or corporation, or conveying any rights or permission to manufacture, use, or sell any patented invention that may in any way be related thereto.

Qualified users may obtain copies of this report from Defense Documentation Center.

Foreign announcement and dissemination of this report is not authorized.

DDC release to OTS is not authorized. The distribution of this report is limited because the report contains technology identifiable with items on the strategic embargo lists excluded from export or re-export under U. S. Export Control Act of 1949 (63 Stat. 7) as amended (50 U.S.C. App. 2020.2031) as implemented by AFR 400-10.

Copies of this report should not be returned to the Research and Technology Division, Wright-Patterson Air Force Base, Ohio, unless return is required by security considerations, contractual obligations, or notice on a specific document.

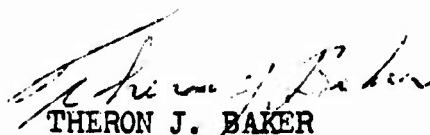
FOREWORD

This report was prepared by the Department of Aeronautics and Engineering Mechanics of the University of Minnesota in compliance with AF Contract No. AF33(657)-11184. The work was initiated under Project No. 6065, "Performance and Design of Deployable Aerodynamic Decelerators," Task No. 606503, "Parachute Aerodynamics and Structures," and covers the period from 15 April 1963 to 1 May 1964.

The work accomplished under this contract was sponsored jointly by U. S. Army Natick Laboratory, Department of the Army; Bureau of Aeronautics and Bureau of Ordnance, Department of the Navy; and the Air Force Systems Command, Department of the Air Force, and was directed by a Tri-Service Steering Committee concerned with Aerodynamic Retardation. The contract was administered by the Recovery and Crew Station Branch, AF Flight Dynamics Laboratory, Research and Technology Division, Wright-Patterson Air Force Base, Ohio. Mr. Rudi J. Berndt and Mr. James H. DeWeese were the project engineers.

This study was accomplished under the direction of Dr. H. G. Heinrich, Professor of Aeronautical Engineering. Mr. Donald Evenson painstakingly carried out the experimental work and data reduction and contributed significantly to the preparation of the report. Mr. Noel A. Dodge conducted most of the experimental work and data reduction for the work presented in the Appendix. A number of graduate and undergraduate students of the University of Minnesota contributed their services, and all these contributions are gratefully acknowledged.

This technical documentary report has been reviewed and is approved.



THERON J. BAKER

Vehicle Equipment Division
AF Flight Dynamics Laboratory

ABSTRACT

An experimental arrangement for determining the apparent moment of inertia of parachute canopy models is described. The rigid canopy models are attached to a simple torsion pendulum and the periods of oscillation of the models and suspension system in air and in water are measured and used to calculate the apparent moment of inertia of the model canopies. The validity of the experimental arrangement was verified by measuring the apparent mass of some simple geometric bodies such as spheres and cubes and comparing the results with known theoretical values. Models of the circular flat, ribbon and ribless guide surface canopy shapes were tested for angular motion about two different axes and the results are presented in nondimensional coefficient form.

Additional results showing the effect of the geometric porosity on the apparent moment of inertia of a ribbon type parachute canopy model are presented in the Appendix.

Previous page was blank, therefore not filmed.

TABLE OF CONTENTS

	PAGE
1. Introduction	1
2. Theory	2
A. General Theoretical Considerations	2
B. Theory of the Experimental Method	3
3. Experimental Equipment	7
A. Trial of Bi-Filar Torsion Pendulum	7
B. Simple Torsion Pendulum Arrangement	7
C. Oscillation Detection System	7
D. Models	9
4. Experimental Procedure and Results	16
A. Experimental Procedure	16
B. Experimental Results	20
5. Conclusions and General Remarks	33
A. Remarks on the Experimental Method	33
B. Discussion of the Experimental Results	34
C. Concluding Remarks	34
<u>Appendix</u> Experimental Investigation of the Effect of Geometric Porosity on the Apparent Moment of Inertia	36
A. Introduction	36
B. Canopy Models and Experimental Arrangement	36
C. Experimental Results and Conclusions	40
D. Concluding Remarks	42
References	43

ILLUSTRATIONS

FIGURE		PAGE
1.	Diagram of Test Frame with a Pair of Spheres as Models	4
2.	Photograph of Test Frame with a Pair of Circular Disks as Models	4
3.	Test Frame and Oscillation Detection Equipment . .	8
4.	Capacitor Mounted on Detection Arm of Test Frame	10
5.	Block Circuit Diagram Showing Basic Components of Capacitance Detection System	10
6.	Test Apparatus with 5" Canopy Model and 1.25" Spheres Attached to Torsion Rod	10
7.	Photographic View of Model Disks, Spheres and Cubes Tested	11
8.	Dimensions and Details of Hemispherical Canopy Model with 1.25" Spheres Attached	12
9.	Dimensions and Details of Circular Flat Canopy Model with 1.25" Spheres Attached	12
10.	Dimensions and Details of Ribbon Canopy Model with 1.25" Spheres Attached	12
11.	Dimensions and Details of Ribless Guide Surface Canopy Model with 1.25" Spheres Attached	12
12.	Photograph of 6" Ribbon Canopy Model	14
13.	Drawing of 6" Ribbon Canopy Model Showing Dimensions (10 Gores)	14
14.	Photograph Showing Two $1\frac{1}{4}$ " Attached Spheres and 2.5" D_p Ribbon Canopies for Confluence Point Tests	15

ILLUSTRATIONS (cont'd)

FIGURE	PAGE
15. Photograph Showing Centrally Mounted 3" Sphere and 2.5" D_p Ribbon Canopies for Confluence Point Tests	15
16. Sample of Trace on Recording Paper Showing Calculation of the Period, T, for 1.5" Diameter Spheres	16
17. Experimental Arrangement for Static Measurement of the Spring Constant	18
18. Apparent Mass Versus Radius Cubed for Circular Disks	21
19. Apparent Mass Versus Displaced Mass for Spheres and Cubes	21
20. 6" Ribbon Canopy Models (6% and 25% Geometric Porosities)	37
21. 6" Ribbon Canopy Model Showing Dimensions for Various Geometric Porosities	37
22. 6" Ribbon Canopy Model as Mounted on Test Frame with Two $1\frac{1}{4}$ " Diameter Steel Spheres	38
23. 2.5" Ribbon Canopy Models (18% and 27% Geometric Porosities)	39
24. 2.5" Ribbon Canopy Model Showing Dimensions for Various Geometric Porosities	39
25. Apparent Moment of Inertia Coefficient ($A_{R,C}$) vs Geometric Porosity for Ribbon Canopy Models Oscillating About Two Different Axes	42

TABLES

TABLE		PAGE
1.	Experimental Data and Calculations of Apparent Mass for Circular Disks	23
2.	Experimental Data and Calculations of Apparent Mass for Cubes and Spheres	23
3.	Experimental Data and Calculations of Apparent Moment of Inertia of Two Hemi- spherical Canopy Models Oscillating About an Axis Through Canopy C. G.	24
4.	Experimental Data and Calculations of Apparent Moment of Inertia of a 6" Hemi- spherical Canopy Model Oscillating About an Axis Through the C. G. of the Included Mass . . .	26
5.	Experimental Data and Calculations of Apparent Moment of Inertia of a 5" Hemi- spherical Canopy Model Oscillating About an Axis Through the C. G. of the Included Mass . . .	26
6.	Experimental Data and Calculations of Apparent Moment of Inertia of a 6" Circular Flat Canopy Model Oscillating About an Axis Through the C. G. of the Included Mass	27
7.	Experimental Data and Calculations of Apparent Moment of Inertia of a 6" Ribbon Canopy Oscillating About an Axis Through the C. G. of the Included Mass	27
8.	Experimental Data and Calculations of Apparent Moment of Inertia of a 6" Ribless Guide Surface Canopy Model Oscillating About an Axis Through the C. G. of the Included Mass . .	28
9.	Experimental Data and Calculations of Apparent Moment of Inertia of a 4" Disk Oscillating About an Axis Through Its Diameter	28
10.	Calculation of the Apparent Moment of Inertia Coefficients for Parachute Models Oscillating About an Axis Through the Confluence Point	30

TABLES (cont'd)

TABLE		PAGE
11.	Summary of Experimental Results of Apparent Mass Tests	29
12.	Summary of Experimental Results of Apparent Moment of Inertia for Canopies Oscillating About an Axis Through the C. G.	32
13.	Summary of Experimental Results of Apparent Moment of Inertia for Canopies Oscillating About an Axis Through the Confluence Point	32
14.	Apparent Moment of Inertia Coefficients for Ribbon Canopies with Various Geometric Porosities Oscillating About an Axis Through the C. G. of the Included Mass	41
15.	Apparent Moment of Inertia Coefficients for Ribbon Canopies with Various Geometric Porosities Oscillating About an Axis Through the Confluence Point	41

SYMBOLS

The notation system adopted for this report is based on a number of basic symbols, representing the primary concepts, supplemented by subscripts and superscripts to further define or restrict the specific meaning. This results in a flexible notation where the association between the symbols and their physical significance is evident and more easily remembered. For clarity and continuity, each combination of symbols involving subscripts or superscripts will be redefined when first introduced in the text.

PRIMARY CONCEPTS

A	Dimensionless moment of inertia ratio
a	Semi-major axis of ellipse
b	Semi-minor axis of ellipse
C	Dimensionless mass ratio
D	Diameter
E	Energy
I	Moment of inertia
K	Torsion rod spring constant
k	Inertia coefficient = kinetic energy/dynamic pressure x displaced volume
L	Distance
l	Side of cube
M	Mass
r	Radius
Re	Reynolds number
S	Surface area
T	Period of oscillation
U	Velocity of body in fluid
$\frac{\partial \phi}{\partial \eta}$	Partial derivative of ϕ with respect to normal direction, directed into the fluid
ϕ	Velocity potential
θ	Angular displacement
Ω	Angular velocity

ρ Density of fluid
 ν Kinematic Viscosity

SUBSCRIPTS

a For tests in air
c For canopy model
d For displaced volume
i For included volume
p For projected diameter
s For sphere
w For tests in water
R Reference mass or moment of inertia based
on system geometry
e For system with models removed

SUPERSCRIPTS

(') For apparent mass and moment of inertia

1. INTRODUCTION

In setting up the dynamic stability equations of a parachute load system and, more generally, in examining the forces and moments acting during unsteady flow conditions, it is necessary to consider not only the actual mass and moment of inertia of the parachute and suspended load but also some additional mass and moment of inertia effects to account for energy exchanges between the parachute and load system on one hand and the fluid medium on the other. These additional mass and moment of inertia effects may become quite important in cases of large instantaneous accelerations and when the air masses involved are large with respect to the parachute mass.

In classical hydrodynamics, it is shown that the effect of the presence of the fluid may be represented by some "additional mass" and "additional moment of inertia," sometimes referred to as the "induced" or "hydrodynamic mass" and "hydrodynamic moment of inertia." Following von Karman's terminology in Ref. 1, the designation "apparent mass" will be used here to represent the "additional mass" for the particular motion under consideration. Similarly, the "apparent moment of inertia" designates the "additional moment of inertia" for the specified angular motion.

The apparent mass and apparent moment of inertia depend on the body shape, the specific motion involved and the density of the fluid in which the motion takes place.

The existing theoretical methods for calculating the apparent mass and moment of inertia can be worked out only in the case of simple geometrical shapes such as spheres and ellipsoids. For parachute canopy shapes, as typified by a hollow hemispherical shell, it is necessary to employ experimental methods.

2. THEORY

A. General Theoretical Considerations

In classical hydrodynamics, a solid body moving in an ideal fluid in steady motion experiences no resistance. This is the so-called "d'Alembert paradox." For unsteady motion, however, the body will be subjected to hydrodynamic forces which are proportional to the instantaneous values of the acceleration and which may be calculated from the known ideal flow.

Lamb, Milne-Thompson and Zahm (Refs. 2, 3 and 4) treat the fundamental concepts and give some information on the apparent mass and moment of inertia effects in the case of simple geometric bodies.

The concepts of apparent mass and moment of inertia are very useful. Their values may be determined from considerations of the energy of the field of flow.

1. Kinetic Energy Relationships

The kinetic energy of an infinite fluid, initially at rest, which is bounded internally by a solid body in potential motion is given by

$$E = -\frac{1}{2} \rho \int_S \phi \frac{\partial \phi}{\partial \eta} dS, \quad (2.1)$$

where E is the fluid kinetic energy,

ρ is the fluid density,

ϕ is the velocity potential, and

$\frac{\partial \phi}{\partial \eta}$ is the velocity along the normal to the boundary directed into the stream.

The integral is taken over the boundary, S , of the region occupied by the fluid flow.

The "apparent mass," M' , is calculated from the kinetic energy by means of the relation

$$E = \frac{1}{2} M' U^2, \quad (2.2)$$

where U is the velocity of the body. Hence,

$$M' = \frac{2E}{U^2} = \frac{-\rho \int_S \phi \frac{\partial \phi}{\partial \eta} dS}{U^2}. \quad (2.3)$$

Reference 2 presents the apparent mass effects in terms of nondimensional inertia coefficients, k , given by

$$k = \frac{\text{kinetic energy}}{\text{dynamic pressure} \times \text{volume of displaced fluid}} . \quad (2.4)$$

The notion of inertia coefficients is a very useful one, but the above definition breaks down in the case of flat plates and thin shells, shapes which are of particular interest in parachute work. To avoid this difficulty, a "reference volume" based on some characteristic dimension of the body, for example the diameter, will be used.

Similarly, in rotational motions the apparent moment of inertia can be determined from energy considerations using the velocity potential of the rotational motion. For an elliptic cylinder, Ref. 3 gives

$$E = \frac{1}{16} \pi \rho \Omega^2 (a^2 - b^2)^2 , \quad (2.5)$$

where a and b are semi-axes of the ellipse and Ω is the angular velocity of rotation of the elliptic cylinder about its axis.

The kinetic energy of rotation is given by

$$E = \frac{1}{2} I' \Omega^2 . \quad (2.6)$$

Hence, the apparent moment of inertia per unit length of rotating cylinder will be

$$I' = \frac{2E}{\Omega^2} = \frac{1}{8} \pi \rho (a^2 - b^2)^2 . \quad (2.7)$$

The general motion of a solid of arbitrary shape involves six degrees of freedom represented by three components of linear velocity and three components of angular velocity. In the quadratic expressions for the energy, there may be six squares and fifteen products of velocity components and therefore 21 hydrodynamic inertia coefficients.

In practical problems the motions may be simplified, as for example in two-dimensional motion, and the bodies considered may have one or more planes of symmetry, thereby reducing the number of inertia coefficients.

B. Theory of the Experimental Method

The experimental method adopted is based on measuring the change in frequency of the body in question when oscillating in air and in water. The actual mass and moment of inertia of the body are the same in both tests, but the apparent mass and the apparent moment of inertia are very different, being proportional to the fluid densities.

In the experimental apparatus used (Figure 1), the models are attached to a stretched wire undergoing small

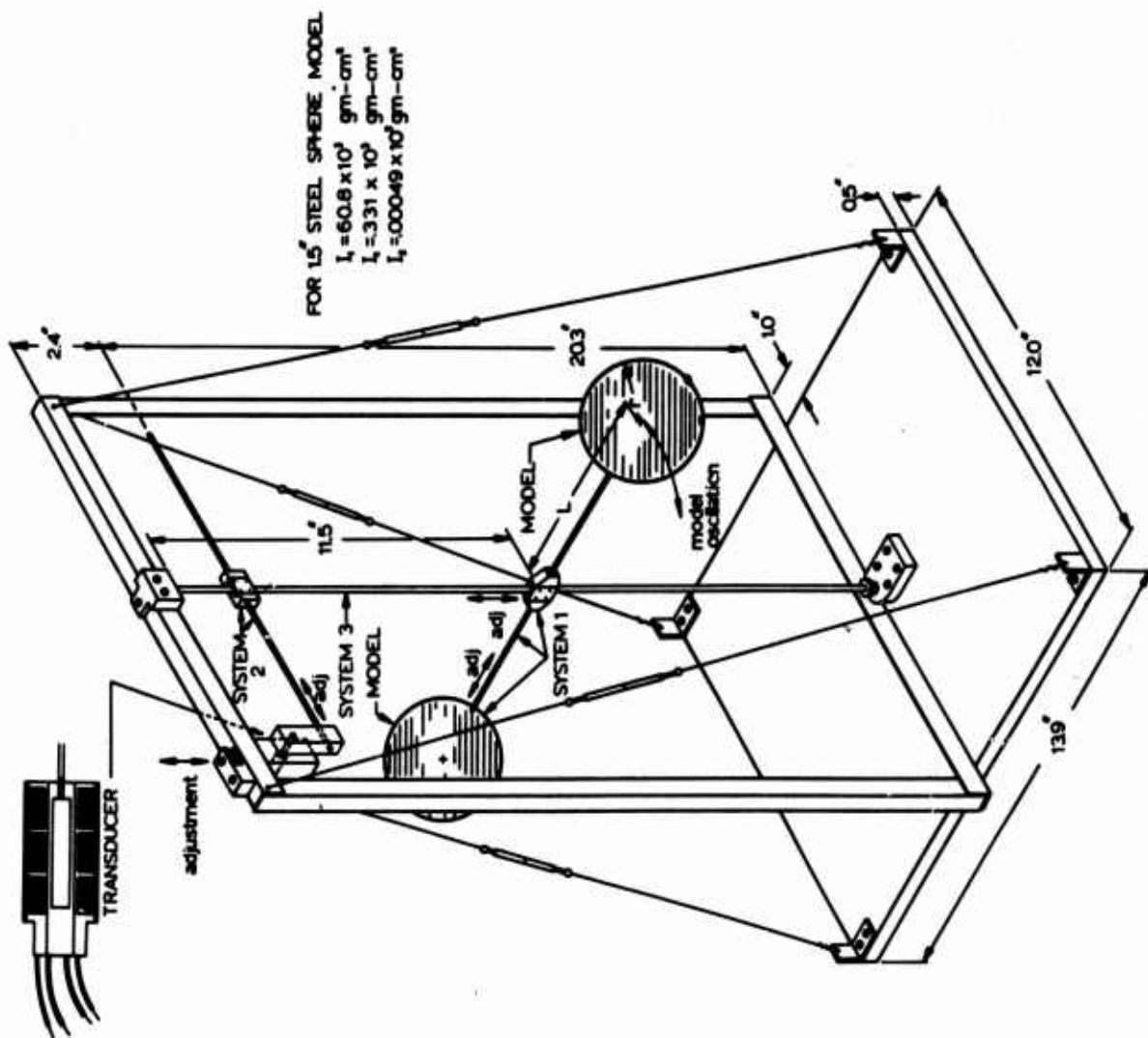


FIG 1. DIAGRAM OF TEST FRAME WITH A PAIR OF SPHERES AS MODELS

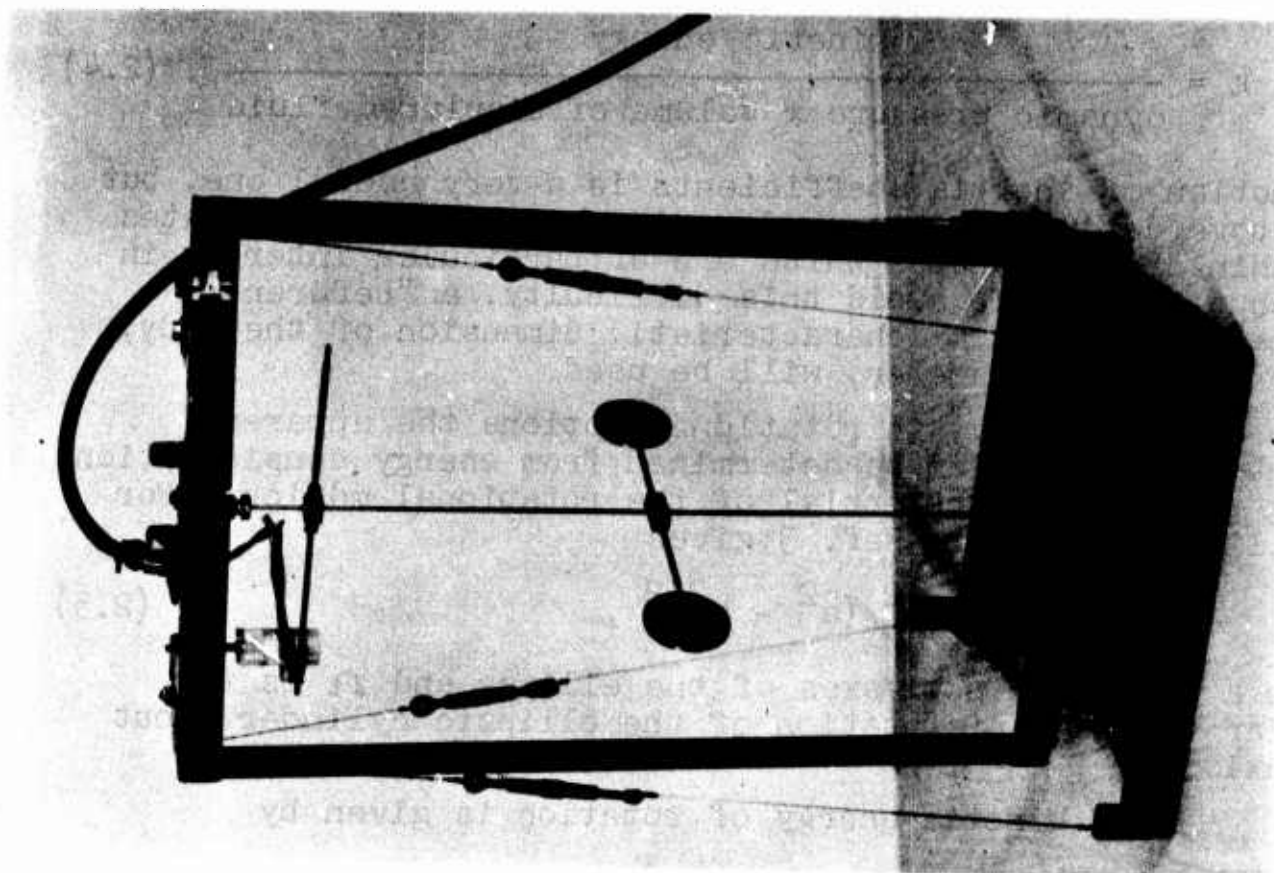


FIG 2. PHOTOGRAPH OF TEST FRAME WITH A PAIR OF CIRCULAR DISKS AS MODELS

torsional oscillations, and the method of attachment of the models is such as to produce the required relative motion for the model.

The period of a torsion pendulum of the type illustrated in Fig 1, held at both ends and oscillating in a fluid, is given by the well known expression

$$T = \frac{2\pi}{\left(\frac{K}{I} - \frac{b^2}{4I^2}\right)^{\frac{1}{2}}}, \quad (2.8)$$

where K = torsional constant of the wire,
 I = effective moment of inertia of the oscillating system, and
 b = damping factor.

The quantity $\frac{b}{2I}$ may be determined experimentally for each configuration and its value incorporated in the data reduction using Eqn (2.8). This greatly complicates the calculations and it is more expedient to choose the torsional constant K and the effective moment of inertia of the oscillating system I in such a way that $\frac{K}{I}$ is considerably larger than $\frac{b^2}{4I^2}$. This can be ascertained experimentally from the small damping of the oscillations as recorded in the trace and illustrated in Fig 16 without the need for the explicit experimental determination of $\frac{b}{2I}$ for each case. This makes it possible to simplify Eqn (2.8) to

$$T = 2\pi \left(\frac{I}{K}\right)^{\frac{1}{2}}. \quad (2.9)$$

If tests for a given model arrangement are conducted in air and in water, then

$$T_a = 2\pi \left(\frac{I_a}{K}\right)^{\frac{1}{2}} \quad (2.10)$$

$$T_w = 2\pi \left(\frac{I_w}{K}\right)^{\frac{1}{2}}. \quad (2.11)$$

The apparent moment of inertia of the oscillating system is given approximately by

$$I_w - I_a = \frac{K}{4\pi^2} (T_w^2 - T_a^2). \quad (2.12)$$

If the apparent moment of inertia of the experimental system without the model attached is designated by I_0 , then the apparent moment of inertia of the model alone will be given by

$$I' = I_w - I_a - I_0 = \frac{K}{4\pi^2} (T_w^2 - T_a^2) - I_0 \quad (2.13)$$

In the case of a symmetric arrangement of two models as shown in Fig 1, the apparent moment of inertia of each model will be one half that given by Eqn 2.13.

It is only necessary to measure the period of oscillation of the system in air and in water, with and without models attached, and to measure the torsional constant of the wire. The latter may be obtained by a separate experiment.

3. EXPERIMENTAL EQUIPMENT

A. Trial of Bi-Filar Torsion Pendulum

Before adopting the experimental set-up shown in Fig 1, another experimental arrangement suggested by Refs 5 and 6 was tried. It consisted essentially of a bi-filar torsion pendulum to which is attached the model under test. By measuring the period of oscillation in air and in a vacuum and allowing for the characteristics of the suspension system, the apparent moment of inertia of the model under test could be calculated. Preliminary tests with a hemispherical cup, oscillating in still air and in the test section of the low density wind tunnel with no flow, gave very little change in the period of oscillation. It was therefore concluded that unfavorable experimental factors such as limited model size, unavoidable friction losses in the suspension system, slight dissymmetry in the model and mounting, etc., made this particular arrangement impractical.

B. Simple Torsion Pendulum Arrangement

The experimental arrangement eventually adopted is similar to that of Ref 7. It consists of a specially designed test frame incorporating a simple torsion pendulum, adjustable mounting arms for the models, and the necessary apparatus for sensing, recording, and timing of the oscillations. Figure 1 shows the main dimensions and design features of the test frame. The torsion rod initially used was a 1/8 inch diameter drill rod, 22 inches long, which was mounted vertically and held fixed at both ends. A small fitting is clamped on the rod at mid-point and carries two threaded 3/32 inch diameter shafts for mounting the models such that the torsional oscillation of the central rod imparts the model motion under investigation.

For symmetry, two identical models mounted on opposite arms are used for the two-body tests. If the motion to be simulated is about an axis through the model, a single model is attached directly to the midpoint of the rod. In other words, the center of gravity of the model system is made to coincide with the midpoint of the torsion rod.

The dimensions of the test frame were chosen so that it could be conveniently immersed in the reservoir tank of the water analogy facility.

C. Oscillation Detection System

1. Inductance Transducer

For the early tests with the 1/8 inch torsion rod, a small linear variable differential transformer was used as a transducer to detect the oscillations. The coil was mounted in a plexiglass fitting attached to the crossarm fitted to the torsion rod near the top. Means were provided for initially

centering the core of the transducer. The transducer is mounted near the upper end of the torsion rod just above the immersion level.

Figure 2 is a photograph of the test frame showing the transducer system and a pair of circular disks attached to the torsion rod. Figure 3 illustrates the amplifying, recording and timing equipment used. This consists of a Model BL-310 Brush Strain Analyser, a two channel Brush pen recorder, a variable frequency oscillator and a Cathode-Ray oscilloscope.

In view of the over-all dimensions of the apparatus and the relatively small range of frequencies of the detection and recording systems and in order to obtain satisfactory experimental measurements, it became necessary to optimize the relationship between the model's mass moment of inertia, its apparent moment of inertia, and the torsion rod spring constant. For the experiments utilizing two solid bodies mounted symmetrically about the torsion rod, the 1/8 inch rod was satisfactory. In later tests using single, thin-shell

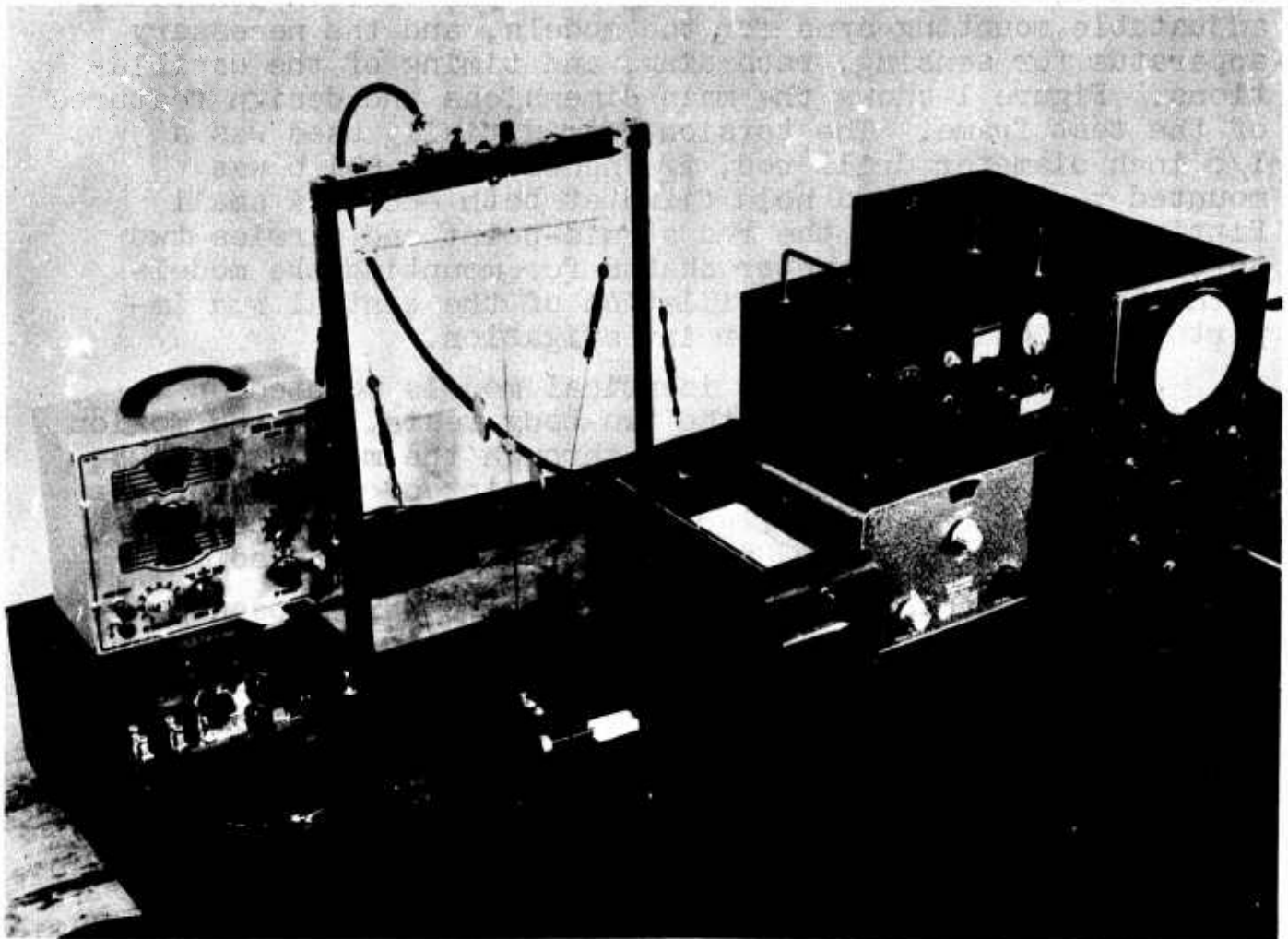


FIG 3. TEST FRAME AND OSCILLATION DETECTION EQUIPMENT

canopies, the oscillations were too small to be measured accurately, because the mass moment of inertia of the model was relatively small. It then became necessary to either reduce the stiffness of the rod or to increase the mass moment of inertia of the canopy model. Since the test frame dimensions limit the size of the canopy models and the use of thicker metal is undesirable for adequate simulation of thin walled canopies, the mass moment of inertia of the models could not be appreciably increased. A 1/16 inch torsion rod was then introduced to reduce the stiffness.

The use of the smaller torsion rod introduced some difficulties in the detection of oscillations by means of the inductance transducer. With the 1/16 inch drill rod as the torsion member, the alignment of core and coil could not be maintained due to the more flexible nature of the smaller rod. It was therefore decided to modify the oscillation detection system.

2. Capacitance Transducer

Capacitance plates mounted symmetrically at the ends of a detection rod were used in conjunction with rigid plates positioned such that the system constituted a variable capacitor. The moving plates and the fixed plates, shown in Fig 4, are mounted 1/8 inch apart. The changing capacitance is detected, amplified and fed into one channel of the two channel Brush pen recorder. Figure 5 diagrammatically shows the basic components of the oscillation detection, amplification and recording system. Figure 6 shows the present instrumentation with a hollow hemispherical model and attached spheres mounted on the torsion rod. This system provides for larger tolerances and easier adjustments than the one using the inductance transducer.

D. Models

1. Two-Body Solid Models

Preliminary tests were conducted using standard geometric shapes in order to compare results with previous theoretical and experimental results. Figure 7 is a photograph of the disks, spheres and cubes that were tested. All of these models were mounted in a manner similar to that of the disks shown in Fig 2.

2. Canopy Models

2.1. Motion about an Axis Through the Center of Gravity

The initial tests on canopy models were for motion about an axis through the center of gravity of the canopies; therefore, single models mounted directly to the torsion rod were used.

For the preliminary tests on rigid canopies, two thin-shelled hemispherical models were used. One model, made

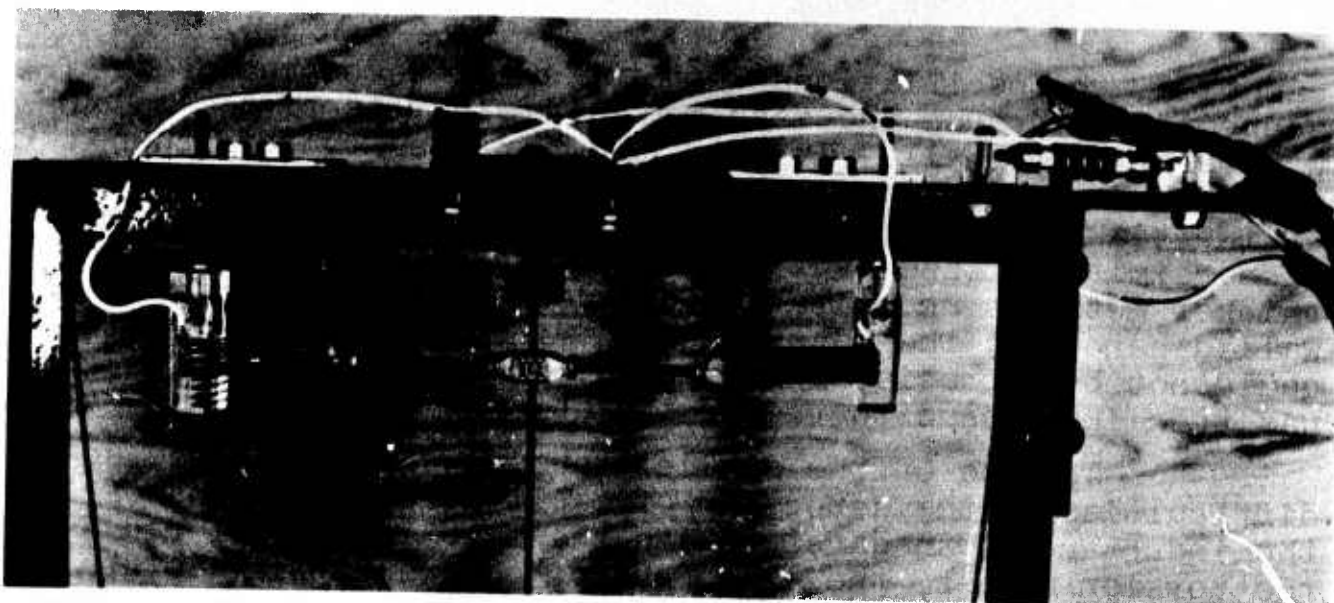


FIG 4. CAPACITOR MOUNTED ON DETECTION ARM OF TEST FRAME

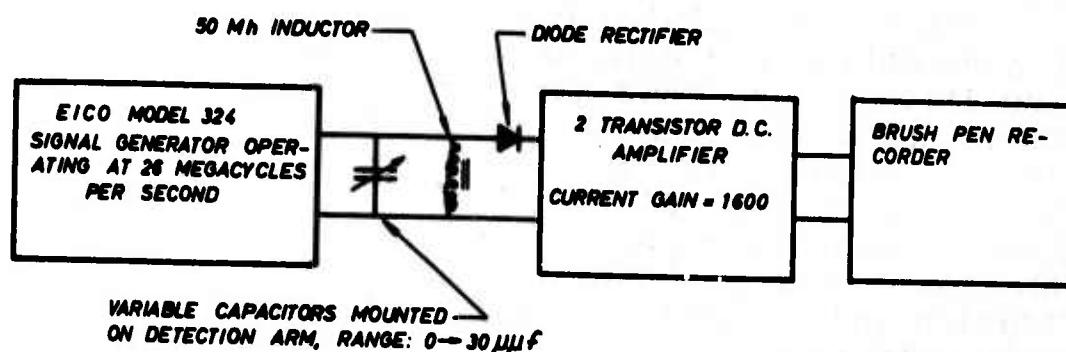


FIG 5. BLOCK CIRCUIT DIAGRAM SHOWING BASIC COMPONENTS OF CAPACITANCE DETECTION SYSTEM

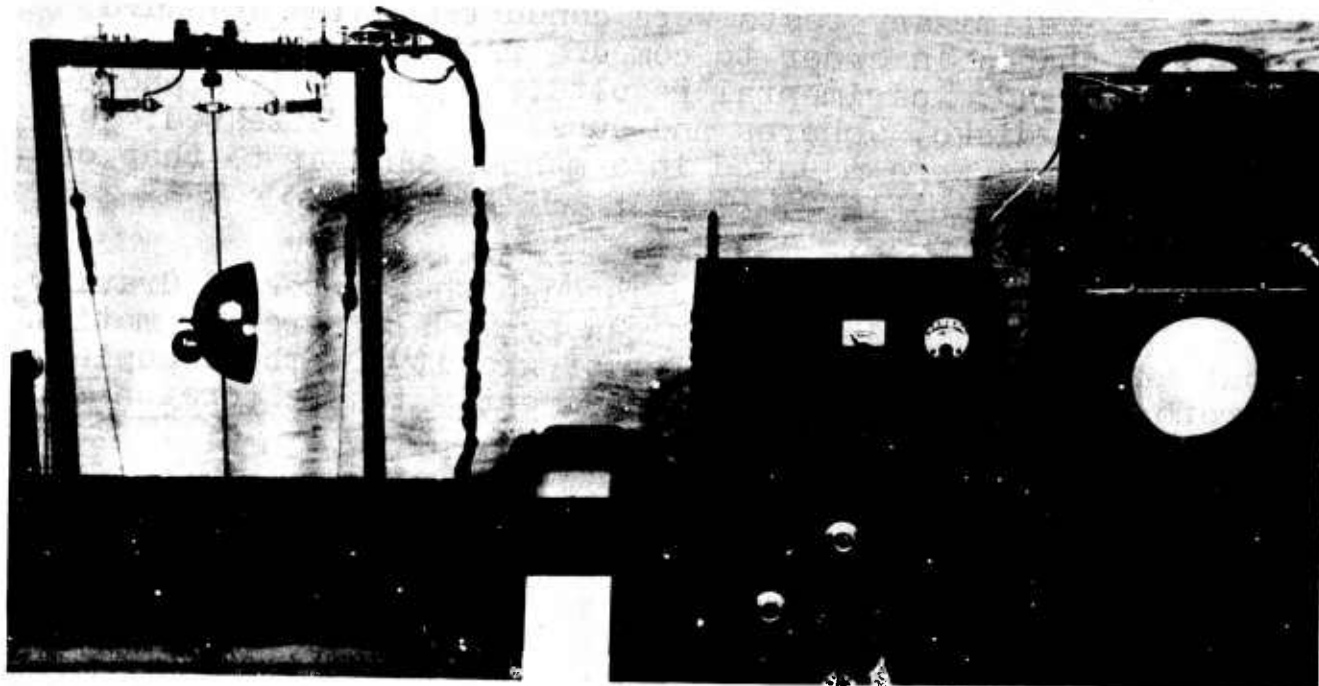


FIG 6. TEST APPARATUS WITH 5" CANOPY MODEL AND 1.25" SPHERES ATTACHED TO TORSION ROD

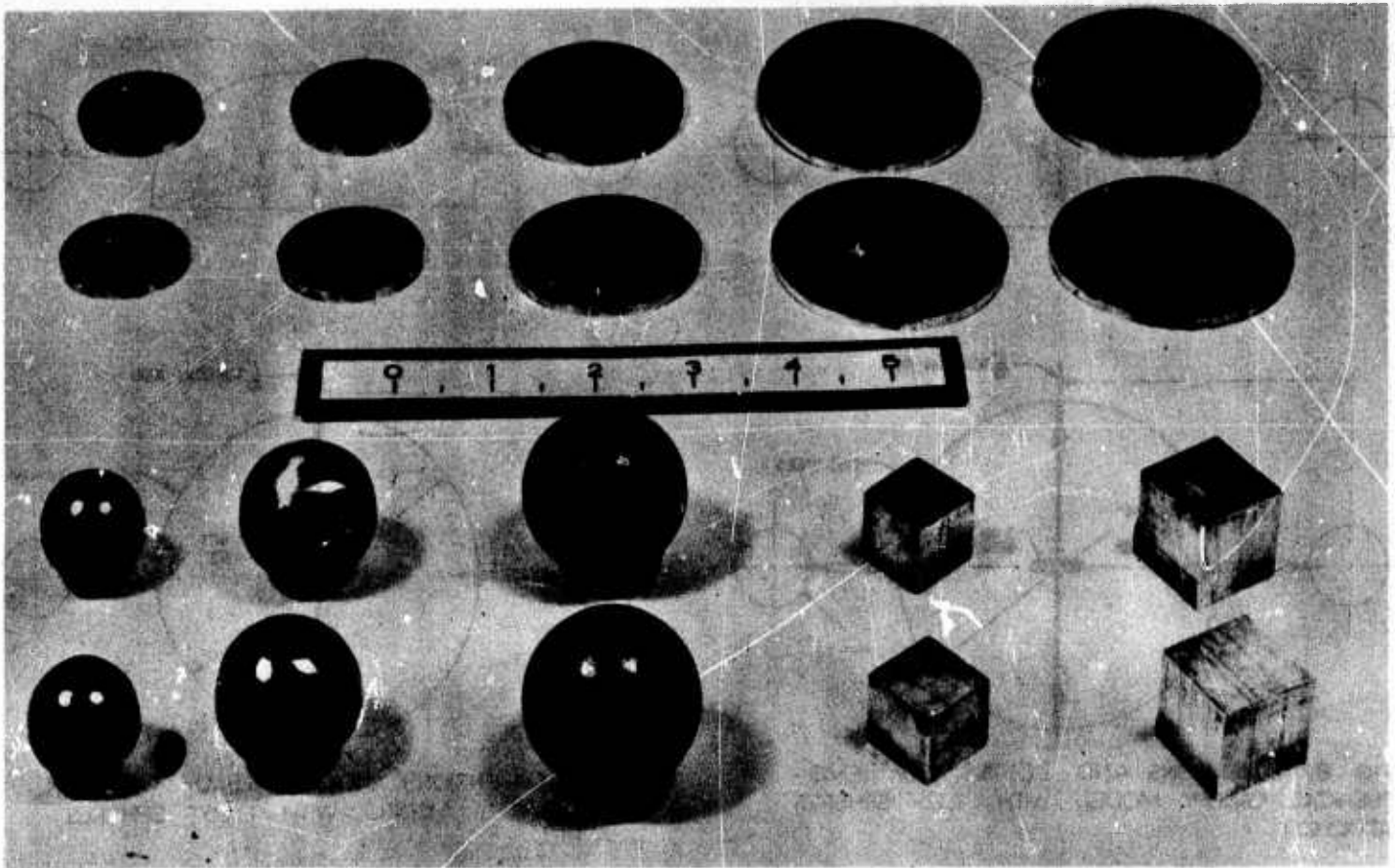


FIG 7 PHOTOGRAPHIC VIEW OF MODEL DISKS, SPHERES,
AND CUBES TESTED

of steel, had an outside diameter of 4 inches and the other model, made of aluminum, had an outside diameter of 6 inches. Both models had wall thicknesses of 0.06 inch. These models oscillated with very little damping in air, but in water the damping was significant, thereby violating our original assumptions. Also, it was difficult to record enough oscillations to get representative periods in water. To overcome these difficulties, solid spheres were mounted on rods protruding from the canopy as shown in Fig 8. These spheres are mounted in such a way as not to interfere with the flow about the canopy; that is, the distance L is large compared with the sphere diameter and the movement of the sphere is small. The real moment of inertia of the system was increased by the addition of these spheres and the damping effect of the water was relatively smaller. The apparent moment of inertia due to the spheres can be accurately accounted for as will be shown later.

Figures 8, 9, 10 and 11 are drawings of the hemispherical, circular flat, ribbon and ribless guide surface

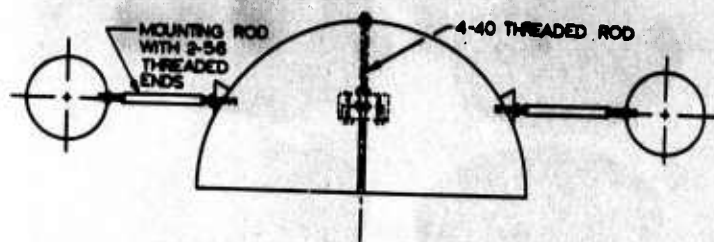


FIG 8. DIMENSIONS AND DETAILS OF HEMISPHERICAL CANOPY MODEL WITH 1.25" SPHERES ATTACHED

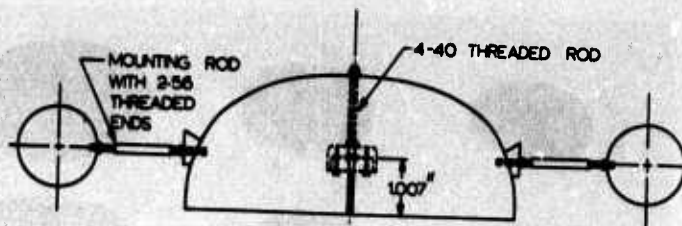
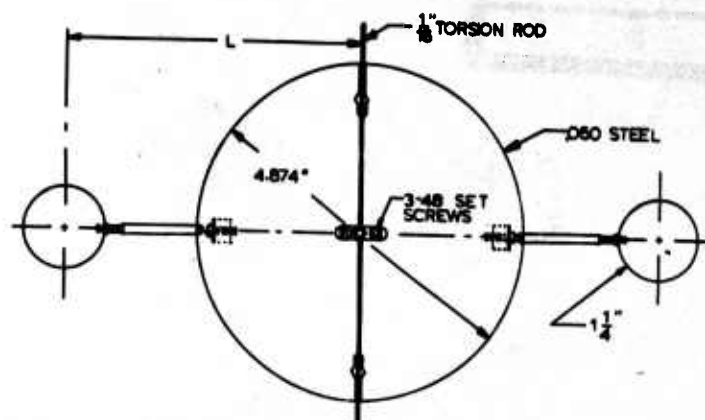


FIG 9. DIMENSIONS AND DETAILS OF CIRCULAR FLAT CANOPY MODEL WITH 1.25" SPHERES ATTACHED

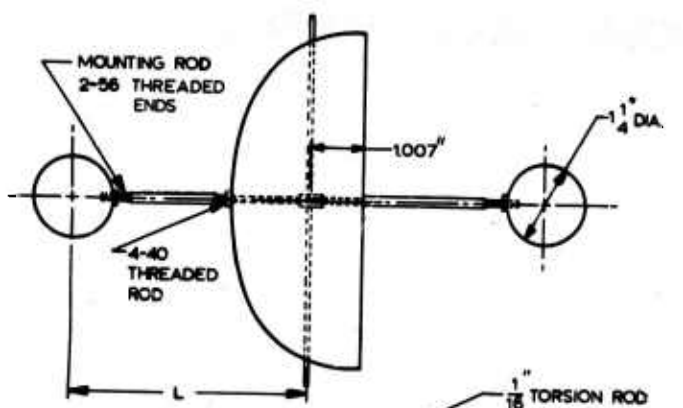
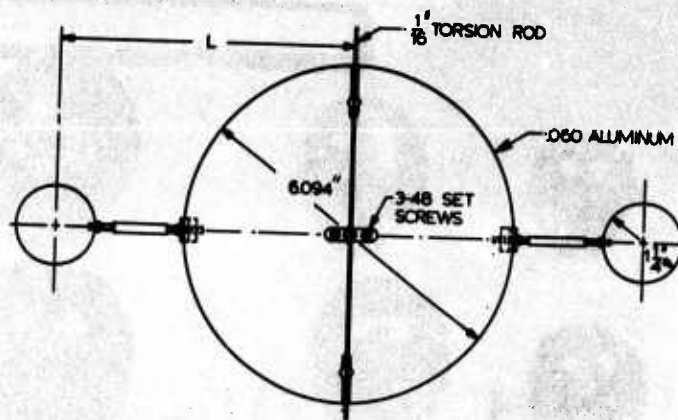


FIG 10. DIMENSIONS AND DETAILS OF RIBBON CANOPY MODEL WITH 1.25" SPHERES ATTACHED

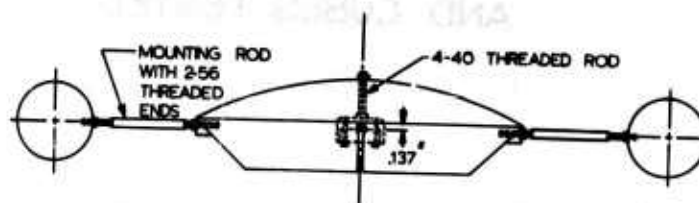
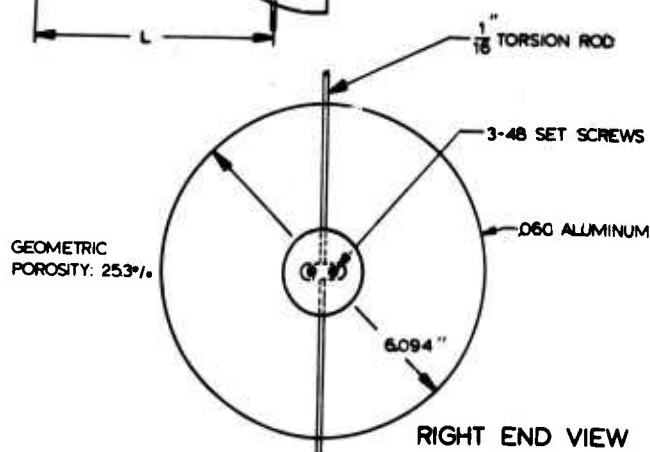
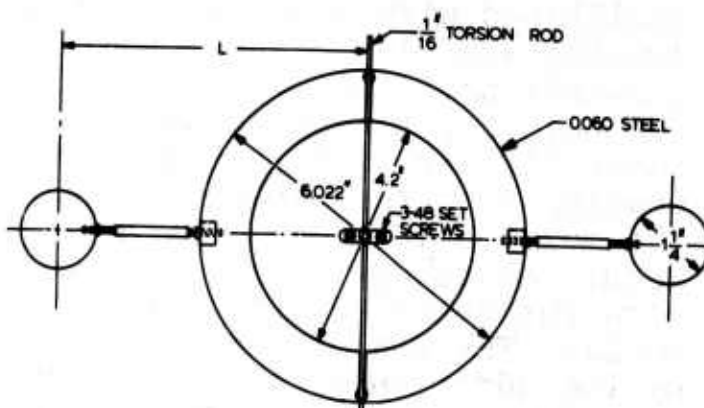


FIG 11. DIMENSIONS AND DETAILS OF RIBLESS GUIDE SURFACE CANOPY MODEL WITH 1.25" SPHERES ATTACHED



canopy models with the additional spheres attached. The hemispherical and ribless guide surface models were made of steel and the circular flat and ribbon models were made of aluminum. All of these models were spun from sheet metal .060" thick. The ribbon canopy model had a geometric porosity of 25.3% and was fabricated by cutting slots in an aluminum circular flat model. Figures 12 and 13 are a photograph and a drawing showing the location and dimensions of the slots in the ribbon model.

2.2. Motion About an Axis Through the Confluence Point

The models which were oscillated about an axis through the confluence point had a projected diameter, D_p , of 2.5" and were spun out of .040" sheet metal. The hemispherical, circular flat and ribbon canopy models were made of aluminum and the ribless guide surface model was made of steel. The geometric porosity of this ribbon canopy is approximately 27%. Drawings of these models are not presented, because they had profiles similar to their 6" diameter counterparts shown in Figs 8 through 11.

Two different test arrangements were used on these canopies. In both cases the leading edge of the canopy skirt was a distance $1.33 D_p$ from the axis of oscillation as shown in Figs 14 and 15. Figure 14 shows the configuration used in the initial tests where two small steel spheres were mounted symmetrically about the torsion rod to increase the inertia of the system in much the same manner as used earlier on the single canopy tests. In later tests a large, centrally mounted sphere was used for the same purpose. The centrally mounted sphere has the advantage of increasing the inertia of the system without increasing the apparent inertia. Figure 15 shows the central sphere arrangement.

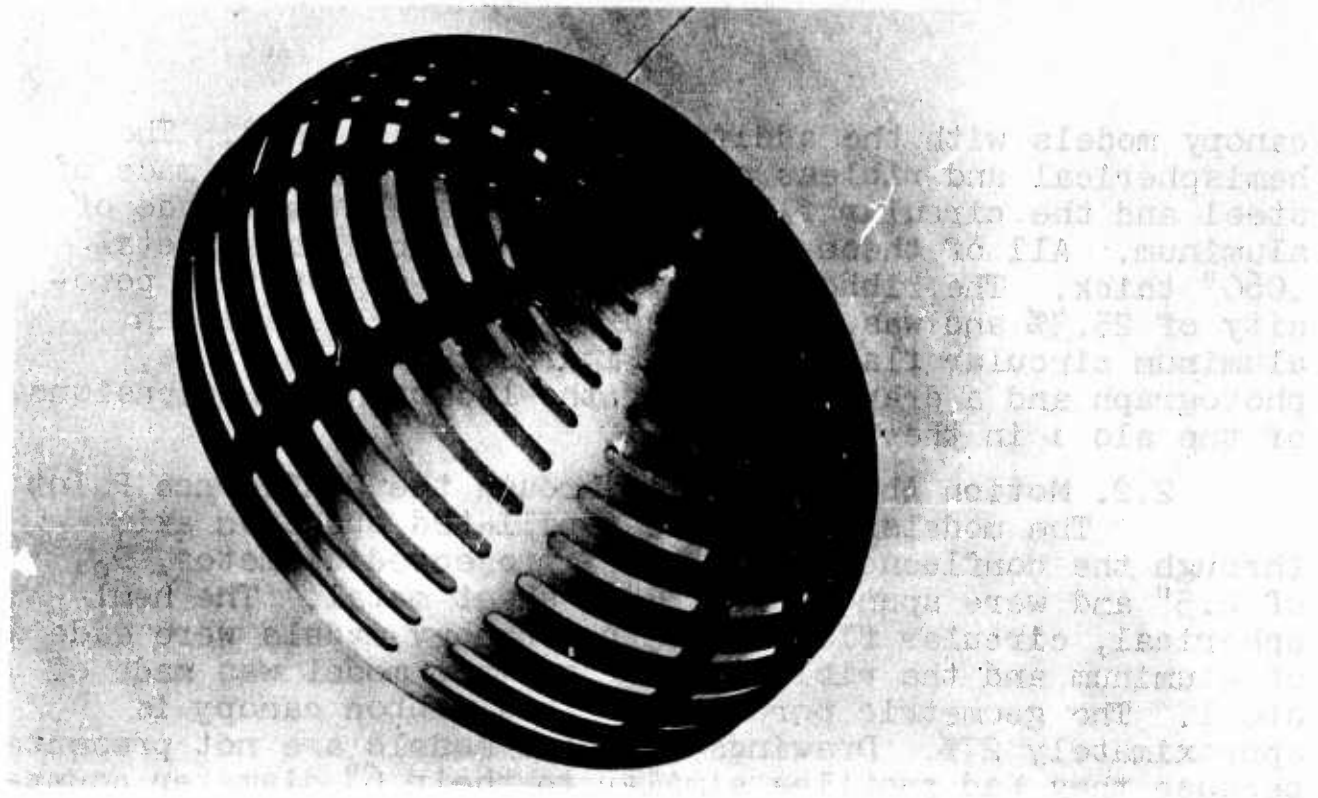


FIG 12. PHOTOGRAPH OF 6" RIBBON CANOPY MODEL

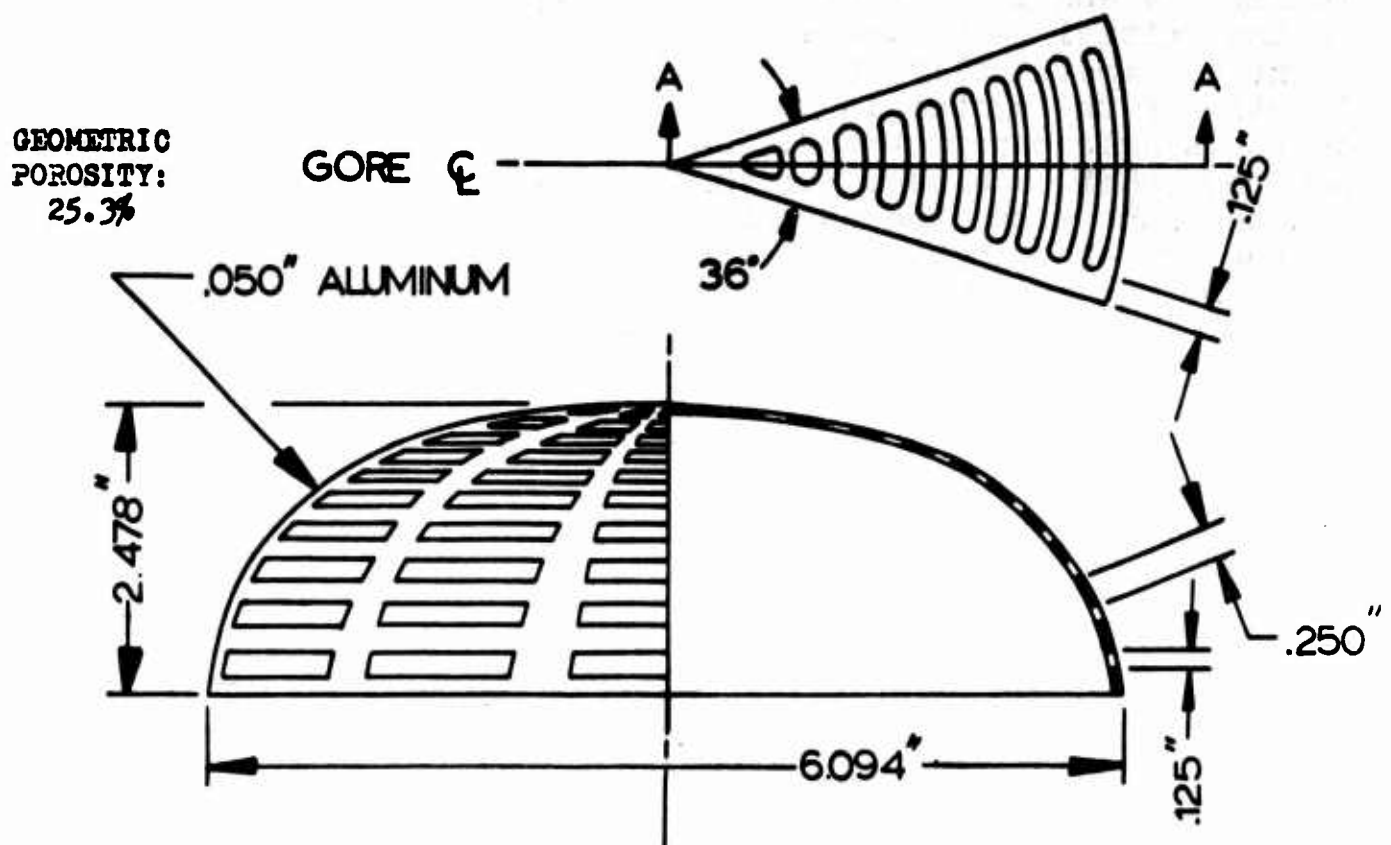


FIG 13. DRAWING OF 6" RIBBON CANOPY MODEL SHOWING DIMENSIONS (10 GORES)

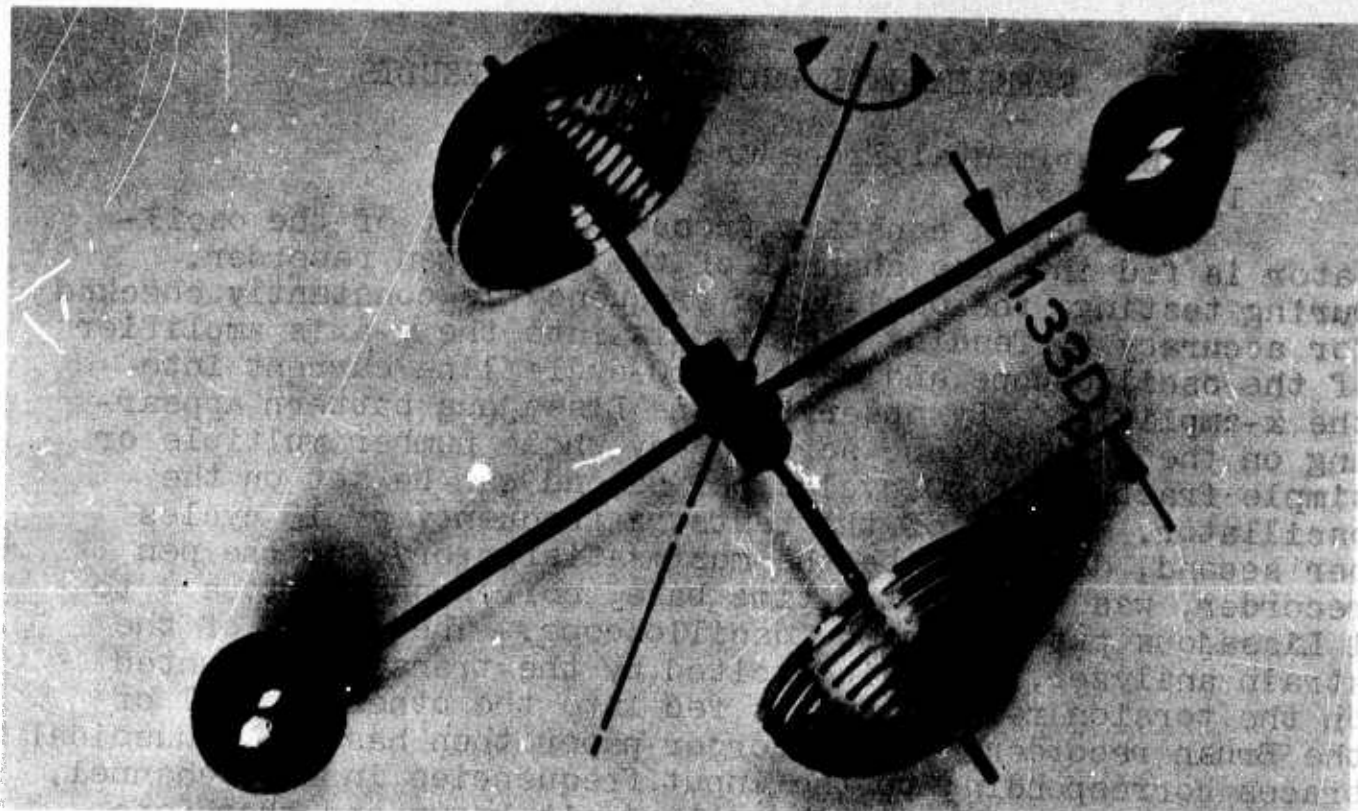


FIG 14. PHOTOGRAPH SHOWING TWO $1\frac{1}{4}$ " ATTACHED SPHERES AND $2.5"$ D_p RIBBON CANOPIES FOR CONFLUENCE POINT TESTS

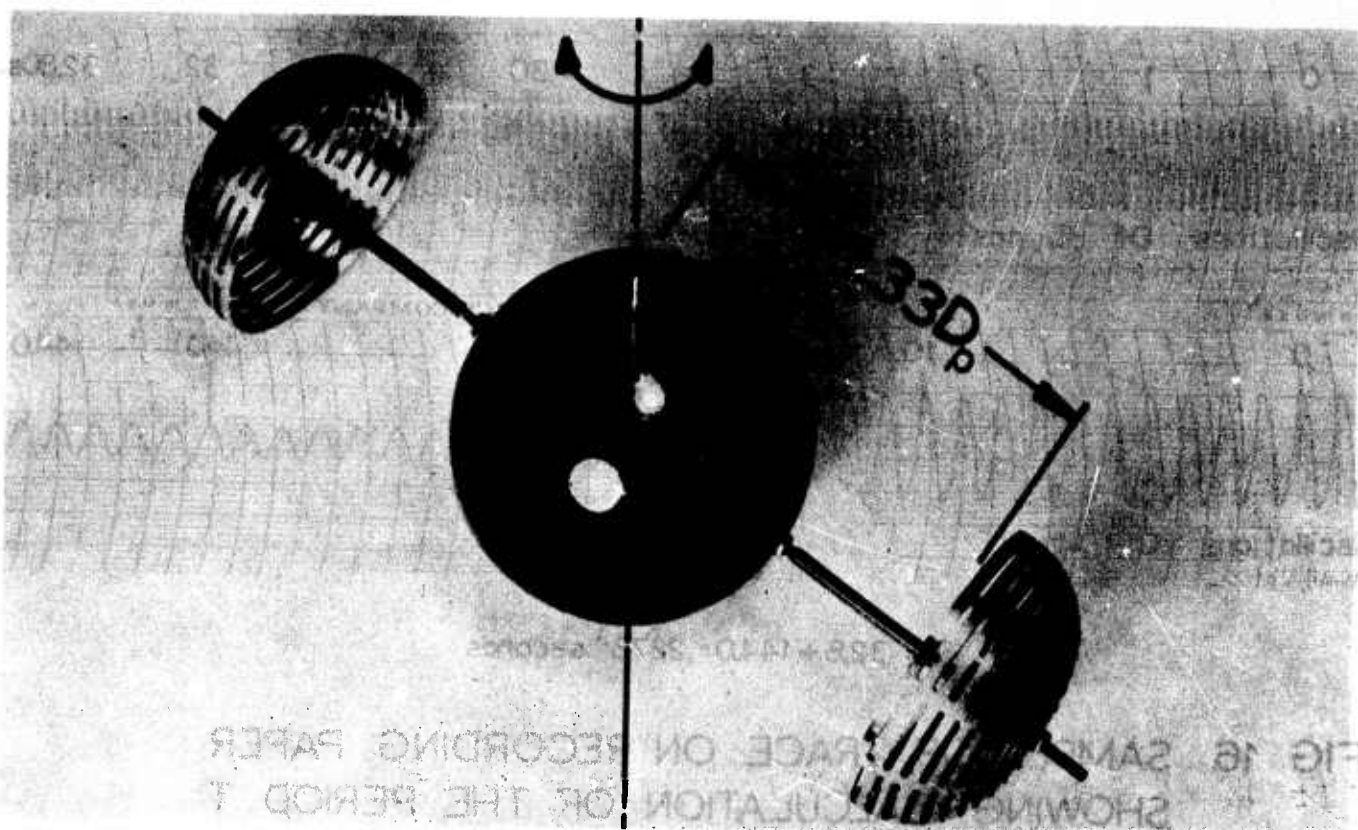


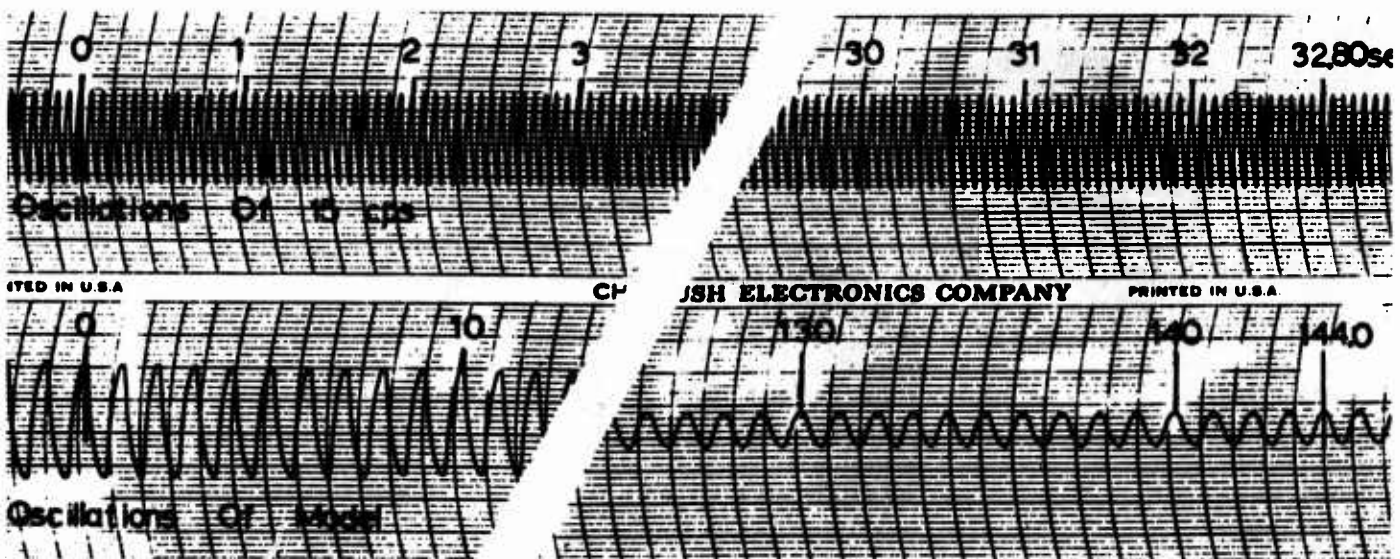
FIG 15. PHOTOGRAPH SHOWING CENTRALLY MOUNTED $3"$ SPHERE AND $2.5"$ D_p RIBBON CANOPIES FOR CONFLUENCE POINT TESTS

4. EXPERIMENTAL PROCEDURE AND RESULTS

A. Experimental Procedure

1. Timing

The known constant frequency output of the oscillator is fed into one channel of the Brush pen recorder. During testing, the oscillator frequency is constantly checked for accuracy by feeding its signals into the y-axis amplifier of the oscilloscope and feeding 60-cycle line current into the x-amplifier. By observing the Lissajous pattern appearing on the oscilloscope screen, any whole number multiple or simple fraction of 60 cycles per second can be set on the oscillator. In all of the tests, a frequency of 15 cycles per second, deemed to be the most satisfactory for the pen recorder, was used as the time base, corresponding to a 4 to 1 Lissajous pattern on the oscilloscope. The output of the strain analyzer, which is excited by the transducer mounted on the torsion rod system, is fed into the other channel of the Brush recorder. The recorder paper then has two sinusoidal traces corresponding to the input frequencies in each channel. The frequency of the time base trace is known and therefore the unknown frequency of the system trace can be determined. Figure 16 shows a sample of recorder paper along with an illustrated calculation of the system's period of oscillation.



$$T = 328 + 1440 = .2278 \text{ seconds}$$

FIG 16 SAMPLE OF TRACE ON RECORDING PAPER
SHOWING CALCULATION OF THE PERIOD T
FOR 1.5" DIAMETER SPHERES

2. Determination of Spring Constant

The determination of the spring constant, K , can be accomplished by either a static or a dynamic test. In the static test, the system was set up as shown in Fig 17, with the angle of deflection determined by the small angle formula

$$\Theta = \frac{\Delta Y}{L} . \quad (4.1)$$

Since the moment arm used in this experiment seemed to bend appreciably, thereby adding its own deflection, another test was conducted to correct for the additional deflection of the moment arm. The moment arm was secured in a rigid vice and reloaded in the same manner as it was when on the torsion rod. The deflection for any given load measured in this test was subtracted from the deflection for the corresponding load on the torsion system. The angles were plotted as a function of the applied torque, with the slope of the line determining the spring constant.

In the dynamic test, the moment of inertia of the system was calculated and the period in air measured. From these values the spring constant was calculated using Eqn 4.2,

$$K = 4 \pi^2 \frac{I}{T^2} , \quad (4.2)$$

where K is the spring constant in dyne-cm. The calculated moment of inertia, I , takes into account systems 1, 2 and 3 shown in Fig 1. System 1, which included the spherical models and the members used to attach the models to the torsion rod, had a calculated moment of inertia of $60.8 \times 10^3 \text{ gm-cm}^2$. System 2, which included the fastener and the rods supporting the moving part of the transducer, had a calculated moment of inertia of $.33 \times 10^3 \text{ gm-cm}^2$. The torsion rod itself, which had a moment of inertia of $.0005 \times 10^3 \text{ gm-cm}^2$, constituted System 3 and was disregarded.

The spring constant determined in this manner compared very well with the constant determined by the static test. For the torsion rod that was tested both statically and dynamically, the spring constant determined by the static test was $45.8 \times 10^6 \text{ dyne-cm}$, while the dynamic test gave $46.0 \times 10^6 \text{ dyne-cm}$. The value of the spring constant determined by the dynamic tests is used in the data reduction because the testing procedure for determining the apparent moment of inertia is similar to that for the determination of the spring constant.

3. Calculation of I' for Two-Body Tests

For the two-body tests, the models were mounted symmetrically on the torsion rod as shown in Fig 1. The

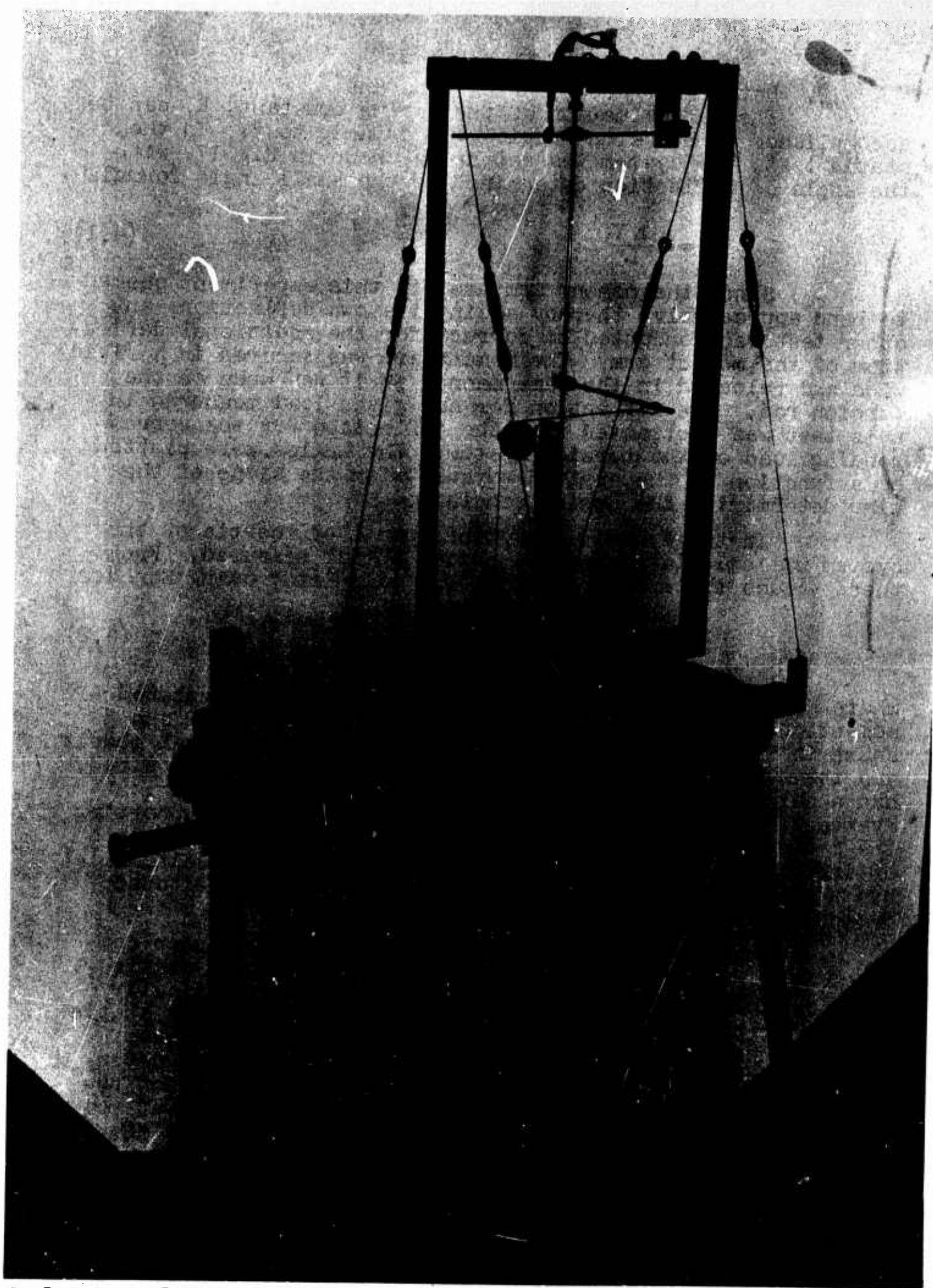


FIG 17. EXPERIMENTAL ARRANGEMENT FOR STATIC MEASUREMENT OF SPRING CONSTANT

apparent moment of inertia of the models was found by measuring the periods of oscillation of the system in air and in water and substituting these values into Eqn 2.13. Under our testing conditions the apparent moment of inertia of the system without models, I'_c , had an estimated value of 31.14 gm-cm² which is negligibly small. With this condition Eqn 2.13 becomes

$$I' = \frac{K}{4\pi^2} (T_w^2 - T_a^2), \quad (4.3)$$

where I' is the apparent moment of inertia of the two models.

4. Calculation of I' for the Single Canopy Tests

In the single canopy tests, it was necessary to account for the effect of the attached spheres. Neglecting mounting apparatus, the apparent moment of inertia of the canopy and the two attached spheres ($I'_c + I'_{2s}$), is obtained by experimental determination of the periods of oscillation in air and water and the use of the relationship

$$(I'_c + I'_{2s}) = \frac{K}{4\pi^2} (T_w^2 - T_a^2), \quad (4.4)$$

which is a modification of Eqn 2.13. The spring constant, K , used in this equation was found by a separate experiment as outlined before. The attached spheres' contribution to the total apparent moment of inertia is designated I'_{2s} , and is found by the equation:

$$I'_{2s} = 2(M'_s L^2) = 2(0.5 M_{d,w} L^2) = M_{d,w} L^2. \quad (4.5)$$

As a check on this method, two hollow hemispherical canopies of the same geometry but different masses were tested. Both canopies had an outside diameter of 5 inches and a wall thickness of .06 inch, but one was made of steel and the other of aluminum. Each canopy was tested with two sets of spheres, one set of $1\frac{1}{4}$ inch steel spheres and one set of $1\frac{1}{2}$ inch steel spheres, and the final results for I'_c were compared.

5. Test Reynolds Number

In the tests, the motion is oscillatory and the velocity of the canopy models fluctuates between zero and a maximum value.

The order of magnitude of the flow Reynolds number will be determined on the basis of an average velocity obtained by dividing the distance traveled in one complete cycle by the period of oscillation. An angle of oscillation of $\pm 2^\circ$ is assumed and the canopy diameter is used as the characteristic length.

The following values are used for the kinematic viscosity ν of water and air at room temperature:

$$\nu_w = 1.23 \times 10^{-5} \text{ ft}^2/\text{sec}$$

and

$$\nu_a = 1.56 \times 10^{-4} \text{ ft}^2/\text{sec}.$$

For angular motion about an axis through the center of gravity of the included mass, the model canopy diameter was 6 inches, and assuming a typical period of 0.9 sec in water and 0.8 sec in air, the calculated Reynolds numbers were:

$$Re_w = 1580 \quad \text{and} \quad Re_a = 140.$$

For the models oscillating about an axis through the confluence point, the model canopy diameter was 2.5 inches, the radial arm from the skirt to the axis of oscillation was $1.33 \times 2.5 = 3.33$ inches, and assuming typical periods of 0.5 sec in water and 0.4 sec in air, the average Reynolds numbers were:

$$Re_w = 1300 \quad \text{and} \quad Re_a = 128.$$

These values justify the assumption of potential flow.

B. Experimental Results

1. Two-Body Tests

The data from tests on the disks is presented in terms of the additional mass, M' , in order to compare our results with those of Ref 7. The working equation used for calculating M' was arrived at by modification of Eqn 4.3. The modified equation has the form

$$I' = 2M'L^2, \quad (4.7)$$

where M' is the apparent mass of one disk and L is the distance from the torsion rod to the center of one of the disks. Therefore,

$$M' = \frac{I'}{2L^2} = \frac{K}{8\pi^2 L^2} (T_w^2 - T_a^2). \quad (4.8)$$

Figure 18 is a graph comparing M' from our tests on disks with experimental and theoretical values found in Ref 7. Our test results lie between previously obtained experimental values and the values calculated by available theory.

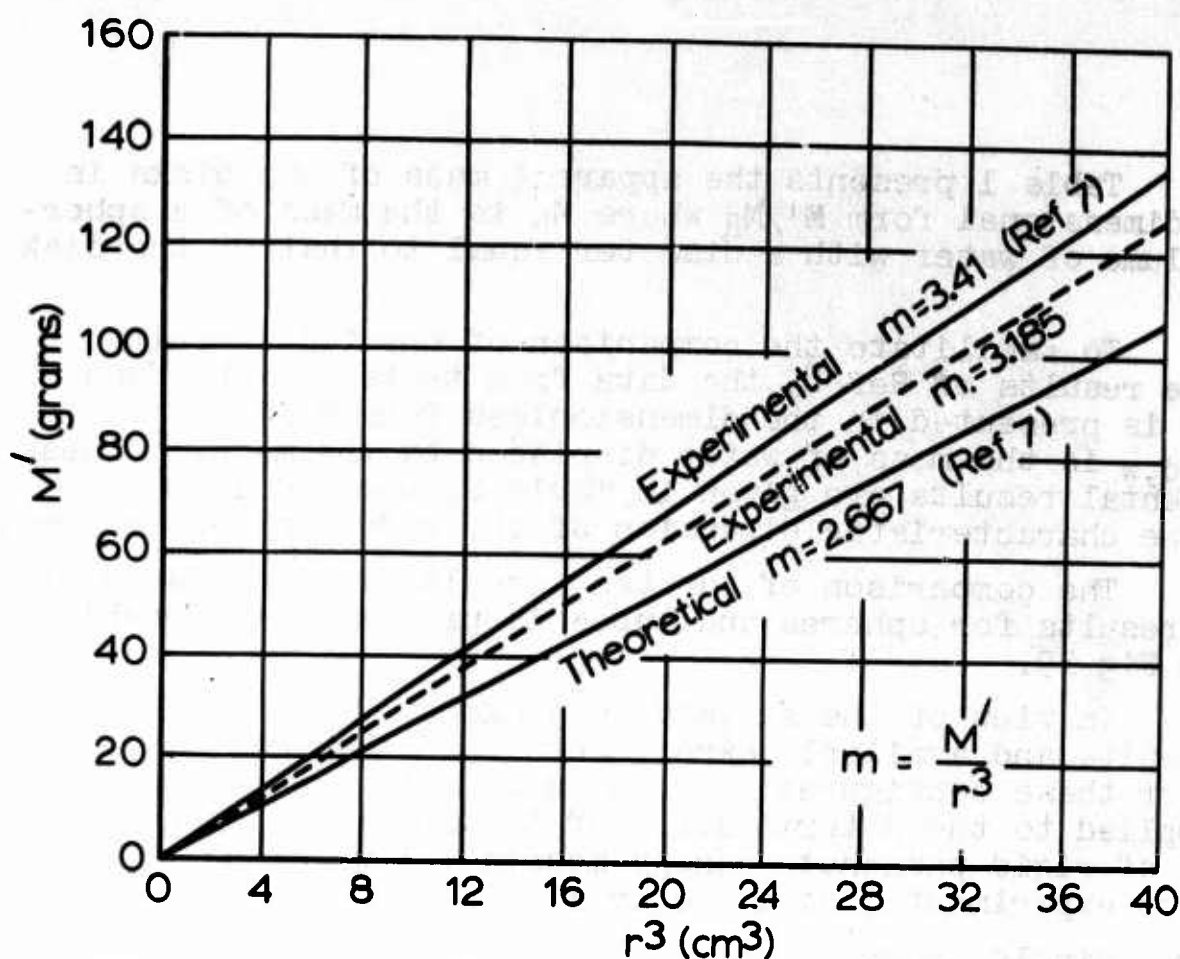


FIG 18. APPARENT MASS VERSUS RADIUS CUBED FOR CIRCULAR DISKS

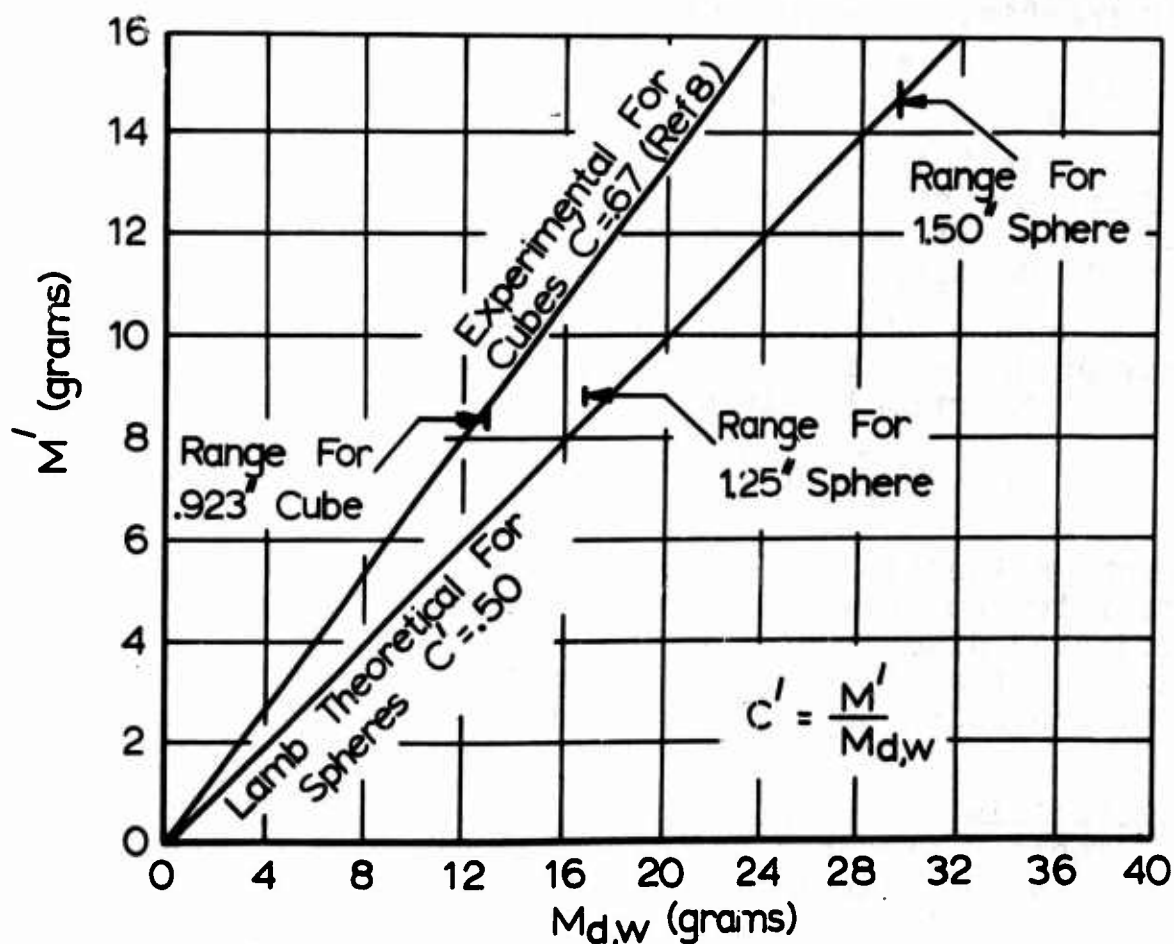


FIG 19. APPARENT MASS VERSUS DISPLACED MASS FOR SPHERES AND CUBES

Table 1 presents the apparent mass of the disks in the nondimensional form M'/M_R where M_R is the mass of a spherical volume of water with a diameter equal to that of the disk tested.

To facilitate the comparison of our test results with the results of Ref 8, the data from tests on cubes and spheres is presented in the dimensionless form $M'/M_{d,w}$, where $M_{d,w}$ is the mass of water displaced by the model. These experimental results are given in Table 2, where Column 1 gives the characteristic dimension of the model in centimeters.

The comparison of our test results and Lamb's theoretical results for spheres and cubes is presented in graphical form in Fig 19.

In view of the satisfactory agreement between our test results and available experimental and theoretical results for these configurations, the same experimental techniques were applied to the determination of the apparent moment of inertia of rigid parachute canopy models for which no theoretical or experimental data are available.

2. Single Canopy Tests

In order to compare the test results for the different canopy configurations, it was necessary to devise a meaningful, dimensionless representation of the apparent moment of inertia. The dimensionless form, defined by

$$A'_{R,c} = \frac{I'_c}{I_R} \quad , \quad (4.9)$$

was adopted. In this representation, I'_c is the apparent moment of inertia of the canopy model and I_R is the moment of inertia of a reference body based on the canopy geometry and the fluid density.

A sphere of water which has a diameter equal to the canopy projected diameter, D_p , was used as a reference. Its moment of inertia is given by

$$I_R = \rho_w \frac{8}{15} \pi \left(\frac{D_p}{2}\right)^5 \quad . \quad (4.10)$$

This moment of inertia was chosen for reference because of its suitability for comparing different canopy shapes of equal projected diameters. It is also applicable to the limiting case of a flat disk. This reference moment of inertia was calculated using the exact diameter of each canopy model tested.

2.1. Oscillation Axis Passes Through the Canopy

Table 3 presents the experimental data and calculations for two 5" diameter hemispherical canopy models, each

TABLE 1. EXPERIMENTAL DATA AND CALCULATIONS OF APPARENT MASS FOR CIRCULAR DISKS

MODEL	① r cm	② t cm	③ L cm	④ L ² cm ²	⑤ $\frac{1}{L^2} \times 10^3$ cm ⁻²	⑥ K × 10 ⁶ dyne-cm	⑦ $\frac{K \times 10^4}{8\pi^2}$ dyne-cm	⑧ $\frac{K}{8\pi^2 L^2}$ dyne/cm	⑨ T _w sec	⑩ T _A sec	⑪ $\frac{T_w^2 - T_A^2}{\text{sec}^2}$	⑫ M' gm	⑬ M _R gm	⑭ $C = \frac{M'}{M_R}$ ⑫/⑬
DISK I	1.920	0.356	11.60	134.6	7.429	47.00	59.53	4422	.1127	.0866	.5207	23.02	29.62	.777
	1.920	0.356	11.60	134.6	7.429	47.00	59.53	4422	.1124	.0867	.5117	22.63	29.62	.764
	1.920	0.356	11.60	134.6	7.429	47.00	59.53	4422	.1127	.0867	.5184	22.92	29.62	.774
DISK II	1.683	0.295	11.49	132.0	7.576	47.00	59.53	4510	.0926	.0710	.3534	15.94	19.95	.799
	1.683	0.295	11.49	132.0	7.576	47.00	59.53	4510	.0926	.0710	.3534	15.94	19.95	.799
	1.683	0.295	11.49	132.0	7.576	47.00	59.53	4510	.0929	.0710	.3584	16.19	19.95	.811
DISK III	2.500	0.335	12.30	151.3	6.609	47.00	59.53	3934	.1650	.1201	1.280	50.36	65.41	.770
	2.500	0.335	12.30	151.3	6.609	47.00	59.53	3934	.1650	.1205	1.270	49.98	65.41	.764
	2.500	0.335	12.30	151.3	6.609	47.00	59.53	3934	.1644	.1203	1.256	49.39	65.41	.755
DISK IV	3.176	0.320	12.98	168.5	5.935	47.00	59.53	3533	.2342	.1622	2.854	100.8	134.1	.752
	3.176	0.320	12.98	168.5	5.935	47.00	59.53	3533	.2353	.1621	2.904	102.6	134.1	.765
	3.176	0.320	12.98	168.5	5.935	47.00	59.53	3533	.2346	.1621	2.876	101.6	134.1	.758
DISK V	3.178	0.312	12.98	168.5	5.935	47.00	59.53	3533	.1942	.0930	2.906	102.7	134.4	.764
	3.178	0.312	12.98	168.5	5.935	47.00	59.53	3533	.1948	.0930	2.906	103.5	134.4	.776
	3.178	0.312	12.98	168.5	5.935	47.00	59.53	3533	.1935	.0932	2.876	101.6	134.4	.755

$$C = \frac{M'}{M_R} = \frac{\frac{K}{8\pi^2 L^2} (T_w^2 - T_A^2)}{\rho_w \frac{4}{3} \pi r^3}$$

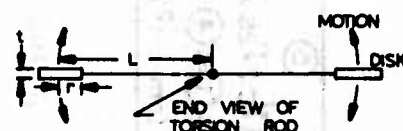


TABLE 2. EXPERIMENTAL DATA AND CALCULATIONS OF APPARENT MASS FOR CUBES AND SPHERES

MODEL	① r cm	② l cm	③ L cm	④ L ² cm ²	⑤ $\frac{1}{L^2} \times 10^3$ cm ⁻²	⑥ K × 10 ⁶ DYNE-CM	⑦ $\frac{K}{8\pi^2} \times 10^4$ DYNE-CM	⑧ $\frac{K}{8\pi^2 L^2}$ DYNE/CM	⑨ T _w SEC	⑩ T _A SEC	⑪ $\frac{T_w^2 - T_A^2}{\text{SEC}^2}$	⑫ M' GM	⑬ M _R GM	⑭ $C = \frac{M'}{M_R}$ ⑫/⑬
CUBE l=2.34cm	—	2.34	10.85	117.7	8.496	47.21	59.79	5080	.1536	.1480	.1689	8.580	12.80	.6703
	—	2.34	10.85	117.7	8.496	47.21	59.79	5080	.1534	.1480	.1628	8.270	12.80	.6462
	—	2.34	10.85	117.7	8.496	47.21	59.79	5080	.1535	.1481	.1629	8.275	12.80	.6465
SPHERE r=1.59cm	1.59	—	11.26	126.9	7.880	47.25	59.84	4715	.1733	.1678	.1876	8.845	16.80	.5265
	1.59	—	11.26	126.9	7.880	47.25	59.84	4715	.1733	.1678	.1841	8.680	16.80	.5167
	1.59	—	11.26	126.9	7.880	47.25	59.84	4715	.1733	.1678	.1876	8.845	16.80	.5265
SPHERE r=1.90cm	1.90	—	11.58	134.1	7.455	46.48	58.87	4389	.2349	.2278	.3285	14.42	29.00	.4972
	1.90	—	11.58	134.1	7.455	46.48	58.87	4389	.2348	.2278	.3238	14.21	29.00	.4900
	1.90	—	11.58	134.1	7.455	46.48	58.87	4389	.2351	.2278	.3379	14.83	29.00	.5114

$$C = \frac{M'}{M_R} = \frac{\frac{K}{8\pi^2 L^2} (T_w^2 - T_A^2)}{M_{d,w}}$$

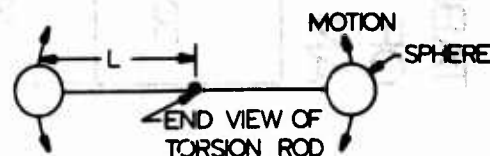
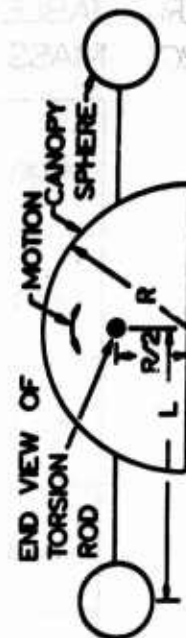


TABLE 3 EXPERIMENTAL DATA AND CALCULATIONS OF APPARENT MOMENT OF INERTIA OF TWO HEMISPHERICAL CANOPY MODELS OSCILLATING ABOUT AN AXIS THROUGH CANOPY C. G.

MODEL CONFIGURATION	① $\frac{K}{4\pi^2} \times 10^{-4}$ (dyne-cm)	②* T_w^2 (sec ²)	③* T_A^2 (sec ²)	④ $(T_w^2 - T_A^2)$ = ② - ③ (sec ²)	⑤ $(I'_C + I'_{2S})$ = ① × ④ (gm-cm ²)	⑥ M_{dW} (gm)	⑦ L (cm)	⑧ I'_{2S} = ⑥ × ⑦ ² (gm-cm ²)	⑨ I'_C = ⑤ - ⑧ (gm-cm ²)	⑩ $\rho_w \frac{8}{15} \pi \left(\frac{D_p}{2}\right)^3$ $I_R \times 10^{-3}$	⑪ $A'_{RC} =$ ⑨/⑩
STEEL											
$1\frac{1}{4}$ " ATTACHED SPHERE	9.00	0.7161	0.6174	0.0987	8,884	16.80	13.85	3,223	5,661	17.29	0.327
$1\frac{1}{2}$ " ATTACHED SPHERE	9.00	1.2099	1.0821	0.1278	11,503	29.00	14.16	5,815	5,688	17.29	0.329
ALUMINUM											
$1\frac{1}{4}$ " ATTACHED SPHERE	9.00	0.6548	0.5605	0.0943	8,488	16.80	13.26	2,953	5,535	17.29	0.320
$1\frac{1}{2}$ " ATTACHED SPHERE	9.00	1.1260	1.0050	0.1210	10,891	29.00	13.57	5,339	5,552	17.29	0.321

*AVERAGE OF 5 RUNS FOR EACH CONFIGURATION

$$A'_{RC} = \frac{I'_C}{I_R} = \frac{K/4\pi^2(T_w^2 - T_A^2) - M_{dW}L^2}{\rho_w \frac{8}{15} \pi \left(\frac{D_p}{2}\right)^3}$$



oscillating about an axis through the center of gravity of the canopies. The results are presented in both the dimensional form I'_c and the nondimensional form $A'_{R,c}$. As shown in Table 3, these canopies were of different material and they were both tested with two sets of spheres. The small variation in I'_c from canopy to canopy may be due to slight experimental inaccuracies in the mounting of the attached spheres. These results appear to justify the method of using attached spheres.

2.2. Oscillation Axis Passes Through C.G. of Included Mass

Tables 4 and 5 give experimental data and calculation of the canopy apparent moment of inertia, I'_c , the reference moment of inertia, I_R , and the nondimensional apparent moment of inertia coefficient, $A'_{R,c}$, for two hemispherical canopy models. These models were oscillated about an axis through the center of gravity of the mass of their included volumes rather than the center of gravity of the canopy shell, as were those presented in Table 3. It is shown that the apparent moment of inertia of the hemispherical canopy is smaller when oscillating about the c.g. of the included mass than when oscillating about the c.g. of the canopy shell.

Table 6 presents the test data and calculated results for a 6" diameter circular flat canopy model oscillating about an axis through the c.g. of the mass of the included volume of the model. The results show satisfactory repeatability and indicate an apparent moment of inertia coefficient of the same order as those for the hemispherical canopies for oscillation about an axis through the c.g. of the included mass.

Table 7 presents the test data and calculated results for a 6" diameter ribbon canopy model oscillating about an axis through the center of gravity of the included mass. These results indicate that the apparent moment of inertia for the circular flat canopy is about five times as great as for the ribbon canopy.

Test data and calculated results for a 6" diameter ribless guide surface canopy model are given in Table 8. The apparent moment of inertia coefficients are approximately equal to those of the hemispherical and circular flat models.

2.3. Oscillation Axis Passes Through C.G. of Disk

Table 9 presents experimental data and calculated results for a 4" diameter disk oscillating about a diameter. The flat disk is the limiting case for canopies oscillating about their enclosed volume c.g. The values of the apparent moment of inertia coefficient, $A'_{R,c}$, for the disk are greater than for the other canopy models as was expected.

3. Two-Canopy Tests: Motion About an Axis Through the Confluence Point

It was necessary to define a reference moment of

TABLE 4. EXPERIMENTAL DATA AND CALCULATIONS OF APPARENT MOMENT OF INERTIA OF A 6" HEMISPHERICAL CANOPY MODEL OSCILLATING ABOUT AN AXIS THROUGH THE C.G. OF THE INCLUDED MASS

6" HEMISPHERE MODEL	① RUN NO	② $\frac{K}{4\pi^2} \times 10^{-4}$ dyne-cm	③ T_w^2 sec ²	④ T_s^2 sec ²	⑤ $(T_w^2 - T_s^2)$ ③ - ④ sec ²	⑥ $(I_s - I_{cm}) \times 10^3$ ② × ⑤ gm-cm ²	⑦ M_{av} gm	⑧ L cm	⑨ $I_{cm} \times 10^3$ ⑦ × ⑧ ² gm-cm ²	⑩ $I_s \times 10^3$ ⑥ - ⑨ gm-cm ²	⑪ $\rho_w \frac{8}{15} \pi (D/2)^5$ ⑩ × ⑤ $I_R \times 10^3$	⑫ $A'_{R,C}$ ⑪ × ⑤
1 $\frac{1}{4}$ " ATTACHED SPHERES	1	8.900	1.1274	.9596	.1678	14.93	16.80	16.07	4.340	10.59	46.50	.228
	2	8.900	1.1278	.9616	.1662	14.79	16.80	16.07	4.340	10.45	46.50	.225
	3	8.900	1.1287	.9551	.1736	15.45	16.80	16.07	4.340	11.11	46.50	.239
	4	8.900	1.1204	.9596	.1608	14.31	16.80	16.07	4.340	9.97	46.50	.214
	Average $A'_{R,C} = .227$											
1 $\frac{1}{2}$ " ATTACHED SPHERES	1	8.900	1.8028	1.5952	.2076	18.48	28.95	16.39	7.778	10.70	46.50	.230
	2	8.900	1.8152	1.6030	.2122	18.89	28.95	16.39	7.778	11.11	46.50	.239
	3	8.900	1.8285	1.6073	.2222	18.78	28.95	16.39	7.778	12.00	46.50	.258
	4	8.900	1.8279	1.6152	.2127	18.93	28.95	16.39	7.778	11.15	46.50	.240
	Average $A'_{R,C} = .242$											

$$A'_{R,C} = \frac{I_s}{I_R} = \frac{K}{4\pi^2} \frac{(T_w^2 - T_s^2) - M_{av} L^2}{\rho_w \frac{8}{15} \pi (D/2)^5}$$

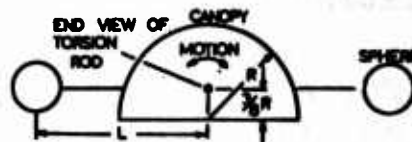


TABLE 5. EXPERIMENTAL DATA AND CALCULATIONS OF APPARENT MOMENT OF INERTIA OF A 5" HEMISPHERICAL CANOPY MODEL OSCILLATING ABOUT AN AXIS THROUGH THE C.G. OF THE INCLUDED MASS

5" HEMISPHERE MODEL	① RUN NO	② $\frac{K}{4\pi^2} \times 10^{-4}$ dyne-cm	③ T_w^2 sec ²	④ T_s^2 sec ²	⑤ $(T_w^2 - T_s^2)$ ③ - ④ sec ²	⑥ $(I_s - I_{cm}) \times 10^3$ ② × ⑤ gm-cm ²	⑦ M_{av} gm	⑧ L cm	⑨ $I_{cm} \times 10^3$ ⑦ × ⑧ ² gm-cm ²	⑩ $I_s \times 10^3$ ⑥ - ⑨ gm-cm ²	⑪ $\rho_w \frac{8}{15} \pi (D/2)^5$ ⑩ × ⑤ $I_R \times 10^3$	⑫ $A'_{R,C}$ ⑪ × ⑤
1 $\frac{1}{4}$ " ATTACHED SPHERES	1	8.900	.7987	.7155	.0832	7.405	16.80	14.76	3.661	3.744	15.24	.246
	2	8.900	.8005	.7144	.0811	7.218	16.80	14.76	3.661	3.557	15.24	.233
	3	8.900	.8010	.7176	.0834	7.423	16.80	14.76	3.661	3.762	15.24	.247
	4	8.900	.8008	.7201	.0807	7.182	16.80	14.76	3.661	3.521	15.24	.231
	Average $A'_{R,C} = .239$											
1 $\frac{1}{2}$ " ATTACHED SPHERES	1	8.900	.8100	.7295	.0855	7.165	28.95	11.35	3.730	3.435	15.24	.225
	2	8.900	.8131	.7281	.0850	7.565	28.95	11.35	3.730	3.835	15.24	.252
	3	8.900	.8127	.7278	.0849	7.556	28.95	11.35	3.730	3.826	15.24	.251
	4	8.900	.8127	.7293	.0834	7.423	28.95	11.35	3.730	3.693	15.24	.242
	Average $A'_{R,C} = .243$											

$$A'_{R,C} = \frac{I_s}{I_R} = \frac{K}{4\pi^2} \frac{(T_w^2 - T_s^2) - M_{av} L^2}{\rho_w \frac{8}{15} \pi (D/2)^5}$$

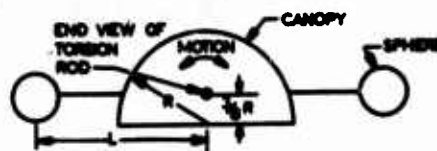


TABLE 6. EXPERIMENTAL DATA AND CALCULATIONS OF APPARENT MOMENT OF INERTIA OF A 6" CIRCULAR FLAT CANOPY MODEL OSCILLATING ABOUT AN AXIS THROUGH THE C. G. OF THE INCLUDED MASS

6" CIRCULAR FLAT MODEL	① RUN NO	② $\frac{K}{4\pi^2} \times 10^4$ dyne-cm	③ T_w^2 sec ²	④ T_c^2 sec ²	⑤ $(T_w^2 - T_c^2)$ sec ²	⑥ $(I_c - I_{25}) \times 10^3$ gm-cm ²	⑦ M_{dw} gm	⑧ L^2 cm ²	⑨ $I_{25} \times 10^3$ gm-cm ²	⑩ $I_c \times 10^3$ gm-cm ²	⑪ $\rho_w \frac{8}{15} \pi (\frac{D_p}{2})^5$ $I_R \times 10^3$	⑫ $A'_{R,c}$ $\frac{⑩}{⑪}$
1 1/4" ATTACHED SPHERES	1	8.900	.6719	.5229	.1490	13.26	16.80	12.58	2.66	10.60	46.50	.228
	2	8.900	.6693	.5249	.1444	12.85	16.80	12.58	2.66	10.19	46.50	.219
	3	8.900	.6648	.5262	.1436	12.78	16.80	12.58	2.66	10.12	46.50	.218
	4	8.900	.6724	.5262	.1462	13.01	16.80	12.58	2.66	10.35	46.50	.223
Average $A'_{R,c} = .221$												
1 1/2" ATTACHED SPHERES	1	8.900	1.0980	.9243	.1737	15.46	28.95	12.90	4.82	10.64	46.50	.229
	2	8.900	1.0900	.9176	.1724	15.34	28.95	12.90	4.82	10.52	46.50	.226
	3	8.900	1.1022	.9264	.1756	15.63	28.95	12.90	4.82	10.81	46.50	.233
	4	8.900	1.0860	.9216	.1644	14.63	28.95	12.90	4.82	9.81	46.50	.211
Average $A'_{R,c} = .225$												

$$A'_{R,c} = \frac{I'_c}{I_R} = \frac{\frac{K}{4\pi^2} (T_w^2 - T_c^2) - M_{dw} L^2}{\rho_w \frac{8}{15} \pi (\frac{D_p}{2})^5}$$

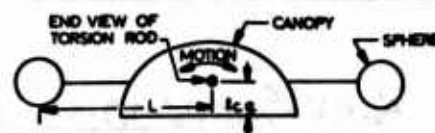


TABLE 7. EXPERIMENTAL DATA AND CALCULATION OF APPARENT MOMENT OF INERTIA OF A 6" RIBBON CANOPY OSCILLATING ABOUT AN AXIS THROUGH THE C. G. OF THE INCLUDED MASS

6" RIBBON MODEL	① RUN NO	② $\frac{K}{4\pi^2} \times 10^4$ DYNE-CM	③ T_w^2 SEC ²	④ T_c^2 SEC ²	⑤ $T_w^2 - T_c^2$ SEC ²	⑥ $(I_c - I_{25}) \times 10^3$ GM-CM ²	⑦ M_{dw} GM	⑧ L^2 CM ²	⑨ $I_{25} \times 10^3$ GM-CM ²	⑩ $I_c \times 10^3$ GM-CM ²	⑪ $\rho_w \frac{8}{15} \pi (\frac{D_p}{2})^5$ $= I_R \times 10^3$	⑫ $A'_{R,c}$ $= \frac{⑩}{⑪}$
GEOM. POROSITY 25.3% 1 1/2" ATTACHED SPHERES	1	9.20	.5776	.5229	.0547	5.03	28.96	96.10	2.78	2.25	46.50	.048
	2		.5764	.5246	.0518	4.77				1.99		.043
	3		.5802	.5259	.0543	5.00				2.22		.048
	4		.5776	.5239	.0537	4.91				2.13		.046
	5		.5776	.5240	.0536	4.93				2.15		.046
	6		.5781	.5230	.0540	4.97				2.19		.047
	7		.5771	.5236	.0535	5.07				2.29		.049
	8		.5755	.5240	.0535	4.92				2.14		.046

AVERAGE $A'_{R,c} = .047$

$$A'_{R,c} = \frac{I'_c}{I_R} = \frac{(\frac{K}{4\pi^2})(T_w^2 - T_c^2) - M_{dw} L^2}{\rho_w \frac{8}{15} \pi (\frac{D_p}{2})^5}$$

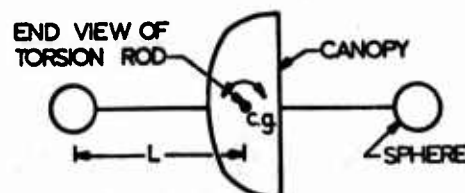


TABLE 8. EXPERIMENTAL DATA AND CALCULATIONS OF APPARENT MOMENT OF INERTIA OF A 6" RIBLESS GUIDE SURFACE CANOPY MODEL OSCILLATING ABOUT AN AXIS THROUGH THE C.G. OF THE INCLUDED MASS

6" RIBLESS GUIDE SURFACE MODEL	① RUN NO	② $\frac{K}{4\pi^2} \times 10^4$ dyne-cm	③ T_w^2 sec ²	④ T_b^2 sec ²	⑤ $(T_w^2 - T_b^2)$ sec ²	⑥ $(I_c' - I_b) \times 10^3$ gm-cm ²	⑦ M_{dw} gm	⑧ L cm	⑨ $I_b' \times 10^3$ gm-cm ²	⑩ $I_c' \times 10^3$ gm-cm ²	⑪ $\rho_w \frac{8}{15} \pi (\frac{D}{2})^5$ $I_R \times 10^3$	⑫ $A_{R,c}$ $\frac{⑩}{⑪}$
1 1/4" ATTACHED SPHERES	1	8.77	.9366	.7783	.1583	13.88	16.80	15.16	3.86	10.02	43.88	.228
	2	8.77	.9442	.7866	.1576	13.82	16.80	15.16	3.86	9.96	43.88	.227
	3	8.77	.9409	.7845	.1564	13.72	16.80	15.16	3.86	9.86	43.88	.225
	4	8.77	.9465	.7862	.1603	14.06	16.80	15.16	3.86	10.20	43.88	.232
	Average $A_{R,c} = .228$											
1 1/2" ATTACHED SPHERES	1	8.77	1.5346	1.3442	.1904	16.70	28.95	15.64	7.08	9.62	43.88	.219
	2	8.77	1.5349	1.3430	.1919	16.83	28.95	15.64	7.08	9.75	43.88	.222
	3	8.77	1.5302	1.3396	.1906	16.71	28.95	15.64	7.08	9.53	43.88	.220
	4	8.77	1.5366	1.3396	.1970	17.28	28.95	15.64	7.08	10.20	43.88	.232
	Average $A_{R,c} = .223$											

$$A_{R,c}' = \frac{I_c'}{I_R} = \frac{K}{4\pi^2(T_w^2 - T_b^2) - M_{dw} L^2} \cdot \frac{8}{15} \pi (D/2)^5$$

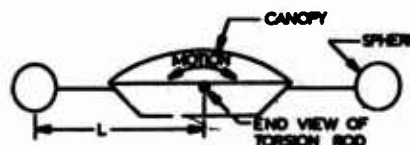
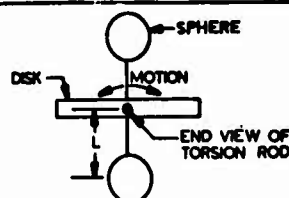


TABLE 9. EXPERIMENTAL DATA AND CALCULATIONS OF APPARENT MOMENT OF INERTIA OF A 4" DISK OSCILLATING ABOUT AN AXIS THROUGH ITS DIAMETER

4" DISK MODEL	① RUN NO	② $\frac{K}{4\pi^2} \times 10^4$ dyne-cm	③ T_w^2 sec ²	④ T_b^2 sec ²	⑤ $(T_w^2 - T_b^2)$ sec ²	⑥ $(I_c' - I_b) \times 10^3$ gm-cm ²	⑦ M_{dw} gm	⑧ L cm	⑨ $I_b' \times 10^3$ gm-cm ²	⑩ $I_c' \times 10^3$ gm-cm ²	⑪ $\rho_w \frac{8}{15} \pi (\frac{D}{2})^5$ $I_R \times 10^3$	⑫ $A_{R,c}$ $\frac{⑩}{⑪}$
1 1/4" ATTACHED SPHERES	1	8.90	.2526	.2229	.0297	2.643	16.80	8.58	1.235	1.408	5.667	.248
	2	8.90	.2528	.2234	.0294	2.617	16.80	8.58	1.235	1.382	5.667	.244
	3	8.90	.2523	.2229	.0294	2.617	16.80	8.58	1.235	1.382	5.667	.244
	4	8.90	.2533	.2232	.0301	2.679	16.80	8.58	1.235	1.444	5.667	.255
	Average $A_{R,c} = .248$											
1 1/2" ATTACHED SPHERES	1	8.90	.02713	.01166	.01547	1.377	0.00	0.00	0.00	1.377	5.667	.243
	2	8.90	.02699	.01164	.01535	1.366	0.00	0.00	0.00	1.366	5.667	.241
	3	8.90	.02696	.01169	.01527	1.359	0.00	0.00	0.00	1.359	5.667	.240
	4	8.90	.02699	.01171	.01528	1.360	0.00	0.00	0.00	1.360	5.667	.240
	Average $A_{R,c} = .241$											

$$A_{R,c}' = \frac{I_c'}{I_R} = \frac{K}{4\pi^2(T_w^2 - T_b^2) - M_{dw} L^2} \cdot \frac{8}{15} \pi (D/2)^5$$



inertia for the confluence point tests in order to present the apparent moment of inertia in dimensionless form. A system incorporating two point bodies each having masses equal to the mass of a sphere of water of diameter D_p and a moment arm equal to the distance from the oscillation axis to the center of gravity of the canopy-enclosed volume was used to calculate the reference moment of inertia, I_{2R} , as shown in Eqn 4.11:

$$I_{2R} = \rho_w \frac{4}{3} \pi \left(\frac{D_p}{2}\right)^3 L^2 (2), \quad (4.11)$$

where

$$L = 1.33 D_p + l_{cg} \quad (4.12)$$

and l_{cg} is the distance from the leading edge of the canopy skirt to the c.g. of its included mass. It should be noted that the measured apparent moment of inertia, I'_c , is for two canopies. Similarly, the reference moment of inertia, I_{2R} , is that of two identical masses.

Table 10 presents the apparent moment of inertia, I'_c , and the nondimensional apparent moment of inertia coefficient, $A'_{R,c}$, for hemispherical, circular flat, ribbon and ribless guide surface models. The data presented in this table is from tests using the central sphere arrangement in which no correction for the apparent moment of inertia of the sphere is required. The results were quite similar for the other test arrangement using two smaller spheres and making the necessary corrections for their apparent inertia.

Table 11 summarizes the experimental results for the apparent mass tests initially conducted on simple bodies.

TABLE 11. SUMMARY OF EXPERIMENTAL RESULTS OF APPARENT MASS TESTS

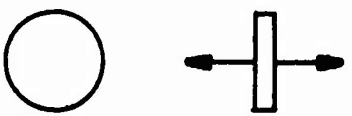


MODEL	REFERENCE MASS	APPARENT MASS COEFFICIENT=C	REMARKS
CIRCULAR DISK 	Displaced Fluid Mass of Sphere of Same Diameter	0.772	Average of Tests on Five Different Sized Disks
CUBE 	Displaced Fluid Mass	0.654	Average of Tests on One Set of Cubes
SPHERE 	Displaced Fluid Mass	0.511	Average of Tests on Two Different Sized Spheres

TABLE 10. CALCULATION OF THE APPARENT MOMENT OF INERTIA COEFFICIENTS FOR PARACHUTE MODELS OSCILLATING ABOUT AN AXIS THROUGH THE CONFLUENCE POINT

MODEL CONFIGURATION	① RUN NO.	② $\frac{K}{4\pi^2} \times 10^4$ DYNE-CM	③ T_W^2 SEC ²	④ T_a^2 SEC ²	⑤ $T_W^2 - T_a^2$ ③-④ SEC ²	⑥ $I'_c \times 10^2$ ②·⑤ GM-CM ²	⑦ $I_{2R} \times 10^2$ GM-CM ²	⑧ A'_{RC} ⑥/⑦
2.5" D _p HEMI-SPHERE CANOPY WITH 3" CENTRAL SPHERE	1	9.20	.2405	.1571	.0834	76.73	249.0	.308
	2		.2414	.1577	.0837	77.00		.309
	3		.2422	.1576	.0846	77.83		.313
	4		.2430	.1586	.0844	77.65		.312
	5	↓	.2427	.1577	.0850	78.20	↓	.314
	Average $A'_{RC} = .311$							
2.5" D _p CIRCULAR FLAT CANOPY WITH 3" CENTRAL SPHERE	1	9.20	.2264	.1607	.0657	60.44	241.3	.250
	2		.2240	.1582	.0658	60.54		.251
	3		.2258	.1591	.0667	61.36		.254
	4		.2256	.1602	.0654	60.17		.249
	5	↓	.2270	.1594	.0676	62.19	↓	.258
	Average $A'_{RC} = .252$							
2.5" D _p RIBBON CANOPY WITH 3" CENTRAL SPHERE	1	9.20	.1712	.1489	.0223	20.52	241.3	.085
	2		.1733	.1501	.0232	21.34		.088
	3		.1734	.1496	.0238	21.90		.091
	4		.1705	.1493	.0212	19.50		.081
	5	↓	.1731	.1495	.0236	21.71	↓	.090
	Average $A'_{RC} = .087$							
2.5" D _p RIBBLESS GUIDE SURFACE CANOPY WITH 3" CENTRAL SPHERE	1	9.20	.2384	.1915	.0469	43.15	228.8	.189
	2		.2373	.1911	.0462	42.50		.186
	3		.2382	.1919	.0463	42.60		.186
	4		.2393	.1909	.0484	44.53		.195
	5	↓	.2351	.1902	.0449	41.31	↓	.181
	Average $A'_{RC} = .187$							

$$A'_{RC} = \frac{I'_c}{I_{2R}} \frac{\frac{K}{4\pi^2} (T_W^2 - T_a^2)}{2L^2 \rho_w \frac{4\pi}{3} \left(\frac{D_p}{2}\right)^3}$$

TABLE 12. SUMMARY OF EXPERIMENTAL RESULTS OF APPARENT MOMENT OF INERTIA FOR CANOPIES OSCILLATING ABOUT AN AXIS THROUGH THE C.G.



Reference Moment of Inertia I_R	Model	Apparent Moment of Inertia Coefficient A_{RC}^I	Remarks
Spherical Fluid Mass of Diameter D_p Centered at Specified C.G. and Oscillating About the Same Axis 	Hemispherical Canopy $D = 5''$	0.324	Axis Through Canopy C.G.
	Hemispherical Canopies $D = 5''$ and $6''$	0.238	Axis Through C.G. of Included Mass 2 Models Tested
	Circular Flat Canopy $D_p = 6''$	0.223	Axis Through C.G. of Included Mass 1 Model Tested
	Ribbon Canopy G.P. = 25.3% $D_p = 6''$	0.047	
	Ribless Guide Surface Canopy $D_p = 6''$	0.226	
	Disk $D = 4''$	0.244	Diametrical Axis 1 Disk Tested

TABLE 13. SUMMARY OF EXPERIMENTAL RESULTS OF APPARENT MOMENT OF INERTIA FOR CANOPIES OSCILLATING ABOUT AN AXIS THROUGH THE CONFLUENCE POINT

Reference Moment of Inertia I_{2R}	Model	Apparent Moment of Inertia Coefficient A_{RC}^I	Remarks
Spherical Fluid Mass of Diameter D_p Centered at Included Mass C.G. and Oscillating About the Same Axis 	Hemispherical Canopy $D_p = 2.5''$.311	Test Results are Averages of Five Runs on Each Model Using Central Sphere Arrangement of Fig. 15
	Circular Flat Canopy $D_p = 2.5''$.252	
	Ribbon Canopy G.P. = 26.6% $D_p = 2.5''$.087	
	Ribless Guide Surface Canopy $D_p = 2.5''$.187	

5. CONCLUSIONS AND GENERAL REMARKS

A. Remarks on the Experimental Method

The experimental apparatus used for measuring the apparent moment of inertia of idealized parachute canopy shapes is basically very simple. Nevertheless, accurate timing of the period of oscillation to within $\pm .0005$ sec is essential, and care is necessary to insure proper symmetry and correct alignment in model mounting. In order to minimize random experimental errors, several runs were made for each configuration and the results were averaged.

The special nature of the flow, characterized by small movements from rest, little damping and a limited Reynolds number range, justifies the assumptions of ideal, incompressible, irrotational flow. The experimental results should therefore approach the theoretical values based on potential flow theory as evidenced by the satisfactory agreement initially obtained with spheres and cubes. The effects of surface friction and flow separation appear to be negligible.

All the tests reported were conducted in air and water only. No need was felt for using other liquids, since previous experimenters had confirmed the existence of a direct relationship between apparent mass and fluid density.

The main dimensions of the apparatus (i.e., the length of the torsion pendulum and size of the test frame) were dictated by practical considerations and more specifically by the dimensions of the water tank. The diameter of the torsion pendulum, model size and additional system inertia were optimized experimentally. It was also ascertained, by experiment, that the effects of the side walls and finite water depth were negligible to the order of experimental accuracy. The 2.5" models were made from .040" thick aluminum or steel and the 6" models were made from .060" thick aluminum or steel. All of the models were spun out to the inflated canopy shapes.

Initially, tests were conducted on identical hemispherical shells made of steel and aluminum and these tests showed no significant effect of the model mass on the experimentally determined apparent moment of inertia. Subsequently, therefore, the model material was selected on the basis of ease of fabrication and reduced cost.

The geometric porosity of the ribbon parachute configuration was represented by corresponding cutouts, but there was no attempt to represent the cloth porosity, the bulging out of the individual gores or the effect of the suspension lines.

B. Discussion of the Experimental Results

The experimental results for the canopies are presented in nondimensional form by using for reference the moment of inertia of a sphere of diameter equal to the projected canopy diameter. This hypothetical sphere is assumed to have the same density as the fluid medium, to be subjected to the same angular motion as the canopy under consideration and to act as one rigid mass.

For angular motion about an axis through the center of gravity of the included mass, the apparent moment of inertia of the circular flat and the ribless guide surface canopies were very nearly the same. The average experimental values for the apparent moment of inertia ratio $A'R_c$ were .223 for the circular flat and .226 for the ribless guide surface types. The average value for the hemispherical canopy was slightly larger at .238. A ribbon canopy model having the same profile as that of the circular flat canopy but with 25.3% geometric porosity showed a very considerable reduction of the value of $A'R_c$ from .223 down to .047, a reduction of about 80% from the value of the circular flat canopy.

For angular motion about an axis through the confluence point assumed to be located at a distance of $1.33 D_p$ from the canopy skirt, the average experimental values for $A'R_c$ were .311 for the hemispherical canopy, .252 for the circular flat, .187 for the ribless guide surface and .087 for the ribbon configuration. Thus, the experimental value of the apparent moment of inertia of the ribbon model is, roughly speaking, a little less than half that of the ribless guide surface model and very nearly one third that of the circular flat parachute model.

C. Concluding Remarks

The need to develop an experimental method for obtaining the apparent moment of inertia of parachute canopies became apparent from a study of the dynamic stability equations of a parachute-store system, which forms a part of our "Investigation of Basic Stability Parameters of Conventional Parachutes." A literature survey failed to reveal any satisfactory analytical or experimental method applicable to rigid hemispherical thin shells representing an idealized form of a parachute canopy.

The experimental apparatus and techniques developed for this purpose and described in this report make possible the determination of the apparent moment of inertia of idealized parachute canopy models having a specified angular motion about a given axis perpendicular to the axis of symmetry.

The experimental values obtained with the proposed method are believed to approximate closely the analytical values that would be obtained on the basis of ideal potential

flow theory. In the case of actual parachute canopies in free flight, the apparent moment of inertia may be significantly different on account of the flexibility and porosity of the parachute cloth and the possible flow separation effects. It is to be expected that the fabric porosity will tend to reduce the apparent moment of inertia while flow separation will tend to increase it.

In spite of possible discrepancies between the results of rigid idealized models and those of full scale flexible parachutes, the model results may be valuable for the purpose of comparing the characteristics of different canopy shapes and providing a reference level from which to introduce corrections to account for flexibility, porosity and flow separation.

The apparatus described and the experimental techniques outlined in this report may be developed and refined if desired. Possible improvements may involve the use of more accurate timing methods, a larger frame with improved suspension, more sophisticated models and special immersion liquid. In the data reduction, a correction may be made for the damping effects at the expense of a much greater complexity in the calculation.

APPENDIX

EXPERIMENTAL INVESTIGATION OF THE EFFECT OF GEOMETRIC POROSITY ON THE APPARENT MOMENT OF INERTIA

A. Introduction

Subsequent to the completion of the experimental work described and the preparation of a draft of a technical report, the Steering Committee adopted the proposal that an additional experimental investigation of the effect of geometric porosity on the apparent moment of inertia be performed and the respective results be presented as an Appendix to this technical report.

B. Canopy Models and Experimental Arrangement

The experimental equipment and test arrangement were the same as described in the main body of the report. The canopy type selected for the porosity tests was the ribbon parachute canopy. Two sizes of canopy models were used, one with $D_p = 6$ inches for tests involving oscillation about an axis through the center of gravity of the included mass and the other with $D_p = 2.5$ inches for the tests involving oscillations about an axis through the confluence point.

The number of slots and the geometric disposition of their centerlines were the same for all models. The different geometric porosities were obtained by progressively increasing the slot widths. The narrowest slots were $1/32$ " wide. These were cut first and the models were then tested. The slot widths were then increased to the next value and the tests were repeated. This procedure resulted in reducing model costs and avoiding slight geometrical irregularities between several models of the same profile but with different porosities.

Figures 20 and 21 illustrate the design details and dimensions of the 6" diameter models. The slot widths used for these models were $1/32$ ", $1/16$ " and $1/8$ ", giving calculated geometric porosities of 6.3, 12.7 and 25.3 per cent, respectively. Figure 22 illustrates the test frame with model canopy and two $1\frac{1}{4}$ " additional spheres attached. The torsion rod used for these tests was the $3/32$ " drill rod.

Figures 23 and 24 illustrate the design details and dimensions of the 2.5" diameter models used for the confluence point tests. The slot widths used for these models were $1/32$ ", $3/64$ " and $1/16$ ", giving calculated geometric porosities of 17.7, 26.6 and 35.4 per cent, respectively. It was not practical to cut slot widths of less than $1/32$ ". For these tests, a symmetric arrangement involving a pair of canopy models was used. It adopts the central 3" diameter

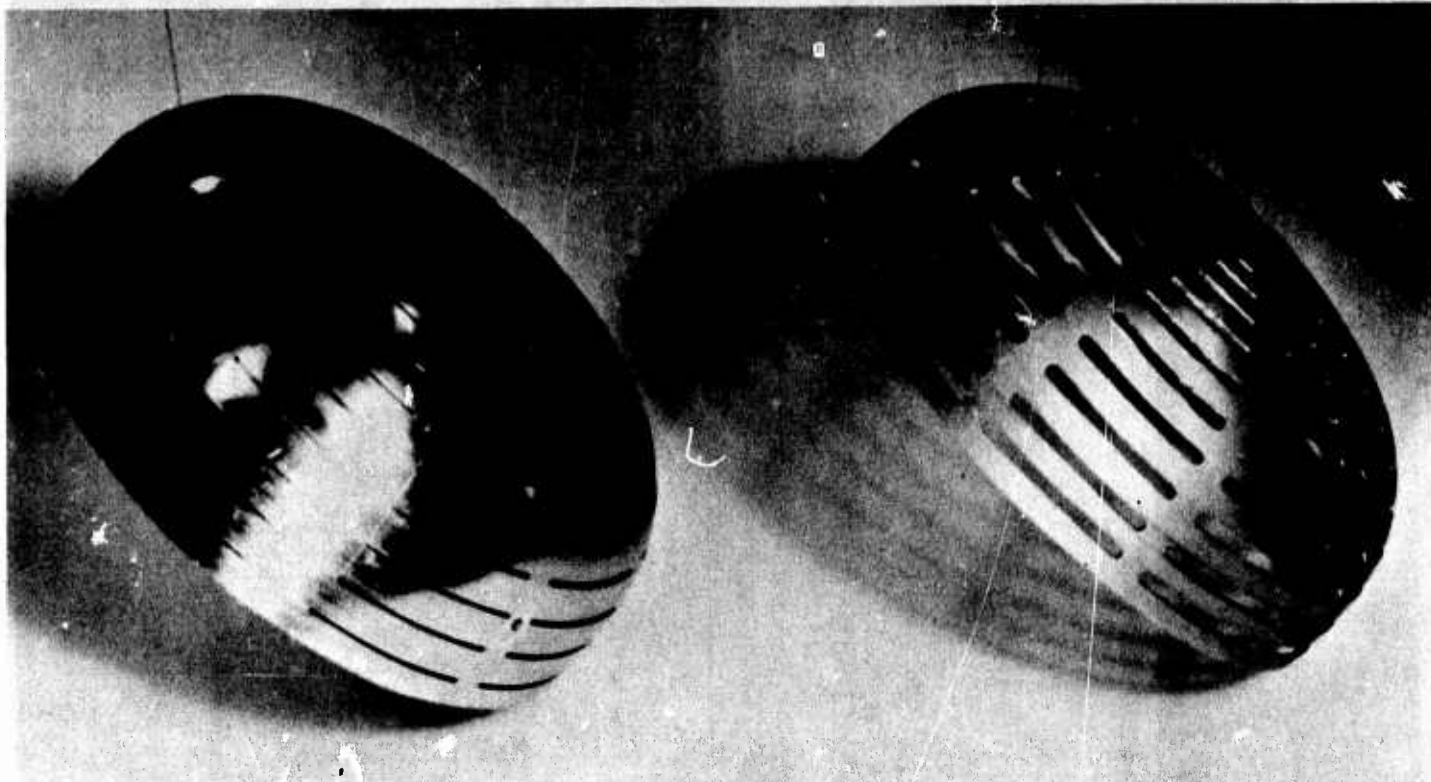


FIG 20. 6" RIBBON CANOPY MODELS (6 % AND 25% GEOMETRIC POROSITIES)

Geom. Porosity	R (in)	S (in)
6.3%	.344	.03125
12.7%	.312	.0625
25.3%	.250	.125

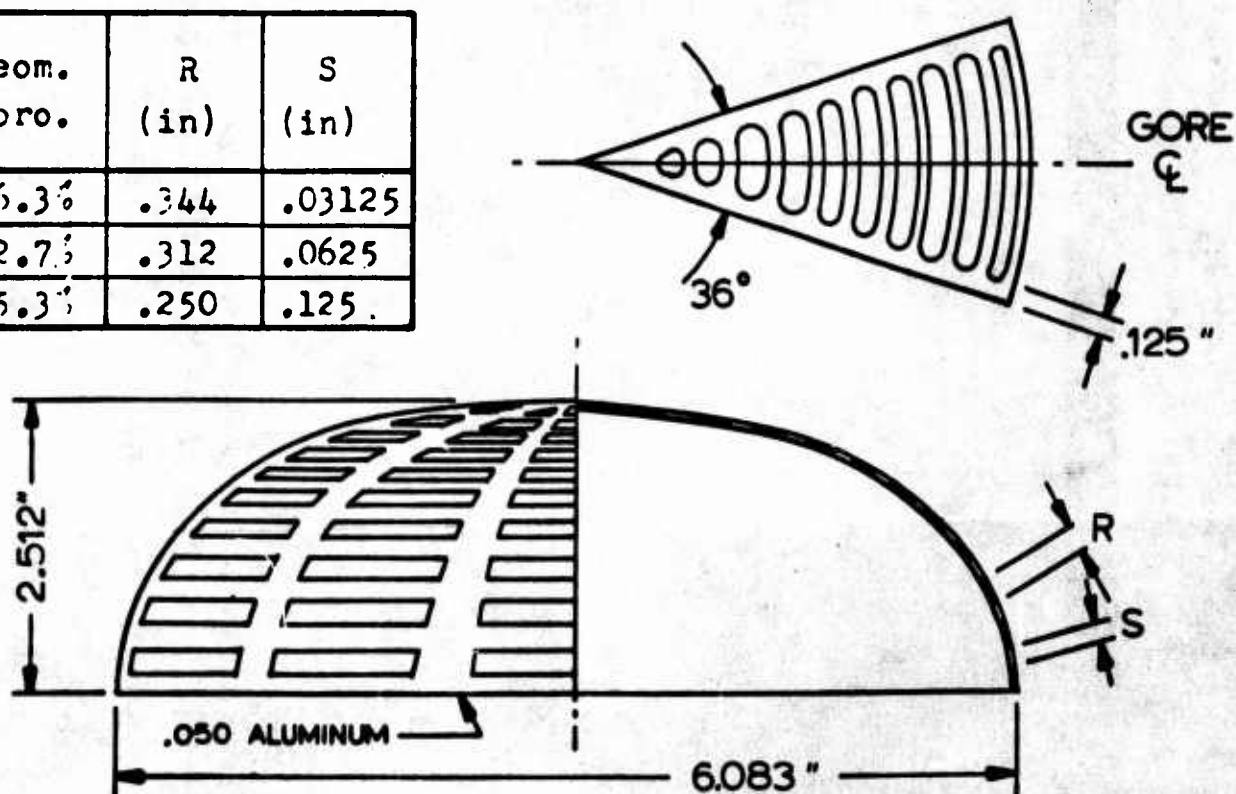


FIG 21. 6" RIBBON CANOPY MODEL SHOWING DIMENSIONS FOR VARIOUS GEOMETRIC POROSITIES

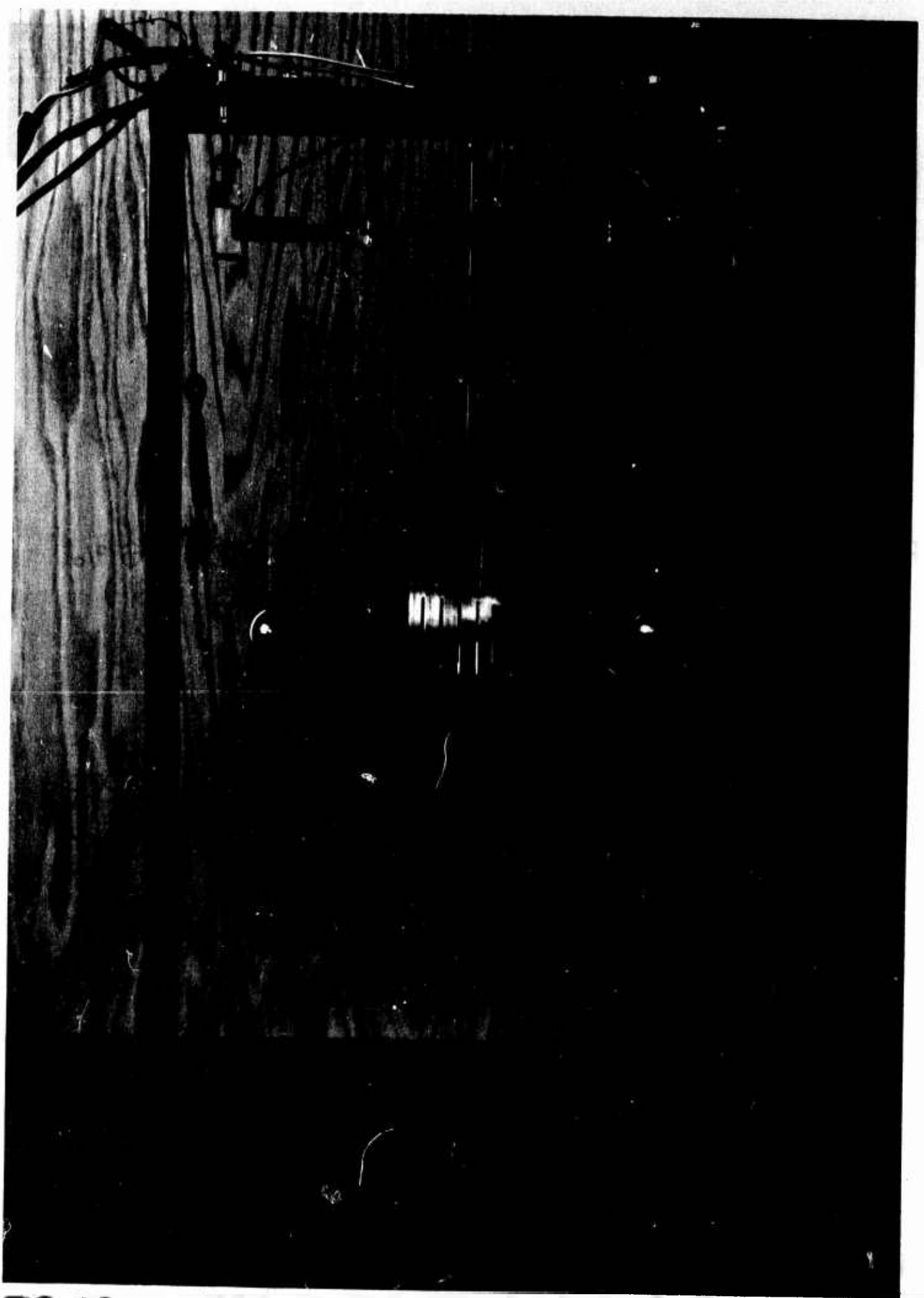


FIG 22. 6" RIBBON CANOPY MODEL AS MOUNTED
ON TEST FRAME WITH TWO $1\frac{1}{4}$ " DIAMETER STEEL
SPHERES

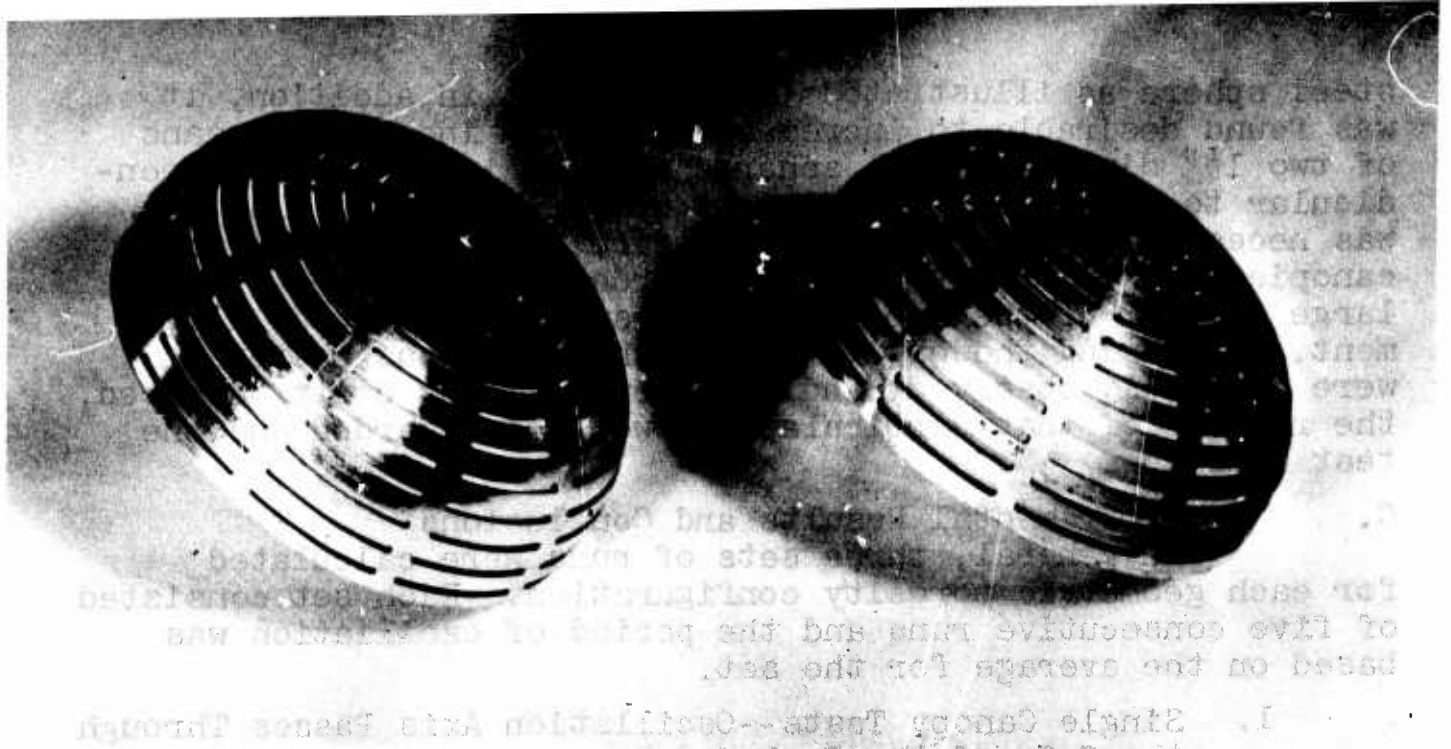


FIG 23. 2.5" RIBBON CANOPY MODELS (18% AND 27% GEOMETRIC POROSITIES)

Geom. Porosity	R (in.)	S (in.)
17.7%	.109	.03125
26.6%	.0937	.0469
35.4%	.0781	.0625

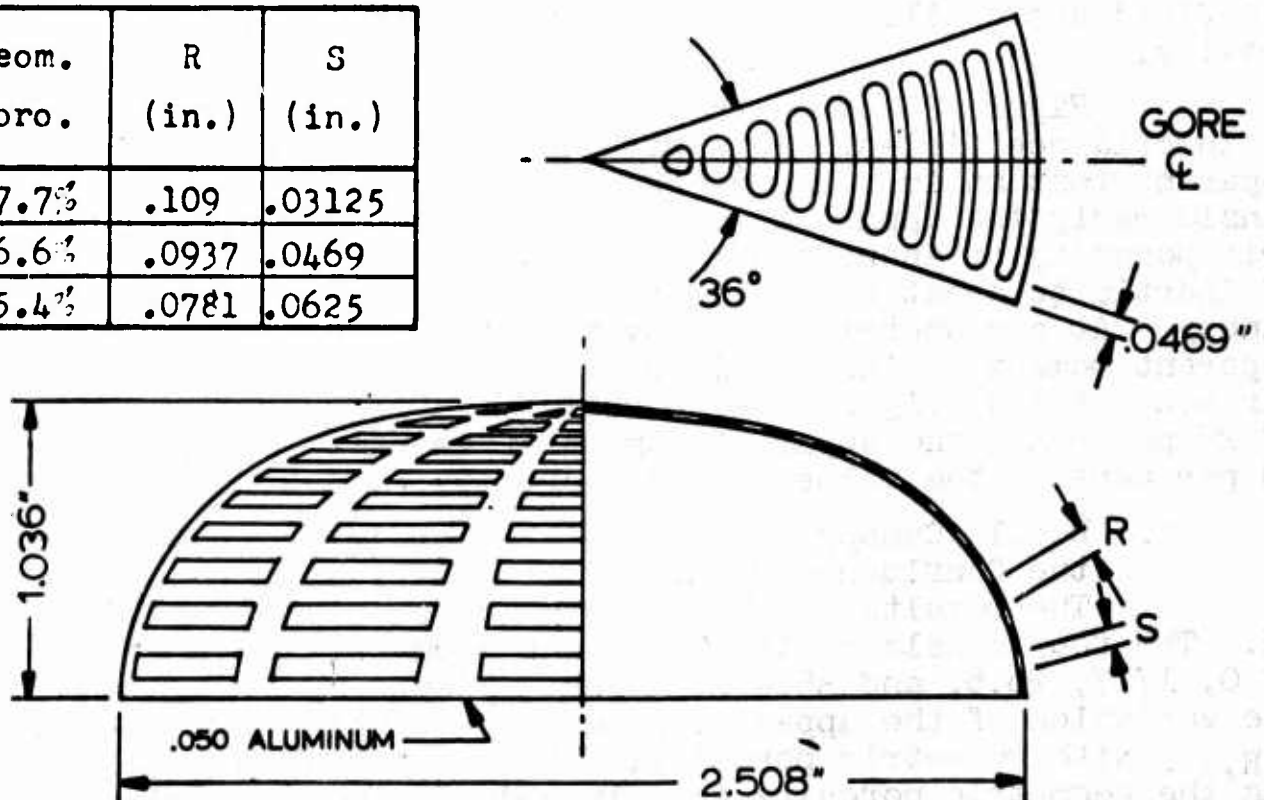


FIG 24. 2.5" RIBBON CANOPY MODEL SHOWING DIMENSIONS FOR VARIOUS GEOMETRIC POROSITIES

steel sphere as illustrated in Fig 15 and, in addition, it was found desirable to increase the system inertia by means of two $1\frac{1}{4}$ " diameter steel spheres mounted in two arms perpendicular to the axis of attachment of the canopy models. It was necessary to exercise special care in aligning the model canopies and auxiliary spheres in order to avoid relatively large scatter of the experimental results due to poor alignment. In timing the oscillations, the Lissajous patterns were carefully observed, and whenever a slight drift occurred, the results of that particular run were disregarded and the test repeated.

C. Experimental Results and Conclusions

In general, three sets of runs were calculated for each geometric porosity configuration. Each set consisted of five consecutive runs and the period of oscillation was based on the average for the set.

1. Single Canopy Tests--Oscillation Axis Passes Through the C.G. of the Included Mass

Table 14 presents the results of tests on four canopy models with geometric porosities of 0, 6.3, 12.7 and 25.3 per cent. The reference moment of inertia, I_R , used for calculating the nondimensional apparent moment of inertia coefficient $A'_{R,c}$ for this case is that of a hypothetical sphere of diameter equal to the projected canopy diameter, D_p , and assumed to act like a solid mass having the density of the fluid and oscillating about an axis through center of gravity.

Figure 25 shows the variation of the apparent moment of inertia coefficient $A'_{R,c}$ with geometric porosity. It is apparent that an increase of geometric porosity reduces considerably the apparent moment of inertia. Thus, a geometric porosity of about 6 per cent reduces the apparent moment of inertia to about 60 per cent of its value for a nonporous canopy. At a geometric porosity of about 13 per cent, the apparent moment of inertia is reduced to approximately 27 per cent of its original value while at a geometric porosity of 25 per cent, the apparent moment of inertia is only about 19 per cent of the value at zero porosity.

2. Double Canopy Tests--Oscillation Axis Passes Through the Confluence Point

The results of these tests are presented in Table 15. The four models tested represent geometric porosities of 0, 17.7, 26.6, and 35.4 per cent. Figure 25 illustrates the variation of the apparent moment of inertia coefficient, $A'_{R,c}$, with geometric porosity. It is apparent that increasing the geometric porosity greatly reduces the apparent moment of inertia. The effect, however, is relatively smaller than for the single canopy tests. A geometric porosity of about

TABLE 14. APPARENT MOMENT OF INERTIA COEFFICIENTS FOR RIBBON CANOPIES WITH VARIOUS GEOMETRIC POROSITIES OSCILLATING ABOUT AN AXIS THROUGH THE C. G. OF THE INCLUDED MASS

MODEL AND GEOMETRIC POROSITY (G. P.)	① SET OF 3 RUNS	② $\frac{K}{4\pi^2} \times 10^3$ DYNE-CM	③ T_w^2 SEC ²	④ T_g^2 SEC ²	⑤ $(T_w^2 - T_g^2)$ ③ - ④ SEC ²	⑥ $(I_c' + I_{2s}') \times 10^3$ ② x ⑤ GM-CM ²	⑦ M_{dw} GM	⑧ L^2 CM ²	⑨ $I_{2s}' \times 10^3$ ⑦ x ⑧ GM-CM ²	⑩ $I_c' \times 10^3$ ⑨ - ⑥ GM-CM ²	⑪ $I_n \times 10^3$ GM-CM ²	⑫ A'_{Rc} ⑩/⑪
$D_p = 6"$ G.P. = 0%	1	89.0	.66960	.52505	.14455	12.8650	16.80	158.3	2.659	10.2060	46.50	.219
	2	89.0	1.0941	.92248	.17157	15.2700	28.95	166.4	4.817	10.4530	46.50	.225
$D_p = 6"$ G.P. = 6.3%	1	329.9	.12327	.09816	.02511	8.2838	16.55	112.1	1.856	6.4277	46.07	.140
	2	329.9	.12229	.09822	.02407	7.9407	16.55	112.1	1.856	6.0846	46.07	.132
$D_p = 6"$ G.P. = 12.7%	1	332.0	.11069	.09678	.01391	4.6181	16.55	112.1	1.856	2.7620	46.07	.060
	2	327.2	.11049	.09635	.01414	4.6266	16.55	109.4	1.812	2.8145	46.07	.060
	3	327.2	.11062	.09647	.01415	4.6299	16.55	109.4	1.812	2.8178	46.07	.061
$D_p = 6"$ G.P. = 25.3%	1	92.0	.57750	.52386	.05364	4.9349	28.96	96.1	2.783	2.1519	46.50	.046
	2	325.6	.10784	.09660	.01123	3.6575	16.55	112.1	1.856	1.8014	46.07	.039
	3	325.6	.10800	.09658	.01143	3.7210	16.55	112.1	1.856	1.8649	46.07	.041

$$A'_{Rc} = \frac{I_c'}{I_n} = \frac{(K/4\pi^2)(T_w^2 - T_g^2) - I_{2s}'}{\rho_w \frac{8}{3} \pi (\frac{D_p}{2})^5}$$

$$I_{2s}' = M_{dw} L^2$$

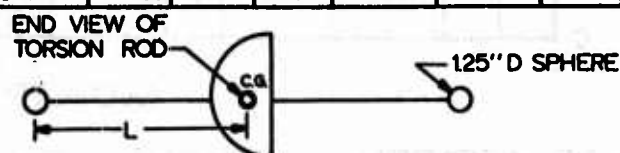


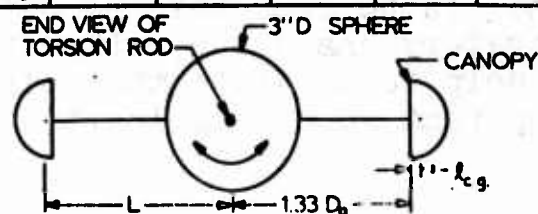
TABLE 15. APPARENT MOMENT OF INERTIA COEFFICIENTS FOR RIBBON CANOPIES WITH VARIOUS GEOMETRIC POROSITIES OSCILLATING ABOUT AN AXIS THROUGH THE CONFLUENCE POINT

MODEL AND GEOMETRIC POROSITY (G. P.)	① SET OF 5 RUNS	② $\frac{K}{4\pi^2} \times 10^3$ DYNE-CM	③ T_w SEC	④ T_g SEC	⑤ T_w^2 SEC ²	⑥ T_g^2 SEC ²	⑦ $T_w^2 - T_g^2$ ⑤ - ⑥ SEC ²	⑧ $(I_c' + I_{2s}') \times 10^3$ ② x ⑦ GM-CM ²	⑨ $I_{2s}' \times 10^3$ GM-CM ²	⑩ $I_n \times 10^3$ GM-CM ²	⑪ A'_{Rc} ⑩/⑪
$D_p = 2.5"$ G.P. = 0%	1	92.0	.4751	.3994	.22576	.15952	.06624	6.094	6.094	24.1	.252
	2	333.0	.3588	.3253	.12874	.10582	.02292	7.032	6.281	24.5	.256
	3	333.0	.3585	.3256	.12852	.10602	.02250	7.493	6.141	24.5	.251
$D_p = 2.5"$ G.P. = 17.7%	1	332.0	.3488	.3235	.12170	.10470	.01700	5.644	4.293	24.5	.175
	2	332.0	.3492	.3231	.12191	.10437	.01754	5.823	4.472	24.5	.183
	3	332.0	.3488	.3234	.12167	.10457	.01710	5.677	4.326	24.5	.17
$D_p = 2.5"$ G.P. = 26.6%	1	332.0	.3402	.3244	.11574	.10524	.01050	3.486	2.135	24.5	.087
	2	335.5	.3392	.3223	.11506	.10420	.01086	3.644	2.292	24.5	.094
	3	335.5	.3393	.3229	.11546	.10426	.01120	3.758	2.406	24.5	.098
$D_p = 2.5"$ G.P. = 35.4%	1	335.0	.3346	.3201	.11200	.10250	.00950	3.182	1.831	24.5	.075
	2	335.0	.3343	.3211	.11178	.10311	.00867	2.904	1.553	24.5	.063
	3	335.0	.3332	.3202	.11102	.10252	.00850	2.848	1.497	24.5	.061

$$* I_{2s}' = 0$$

$$A'_{Rc} = \frac{I_c'}{I_{2s}'} = \frac{K/4\pi^2 (T_w^2 - T_g^2) - I_{2s}'}{2 I_{2s}' \frac{8}{3} \pi (\frac{D_p}{2})^5}$$

$$I_{2s}' = M_{dw} L^2$$



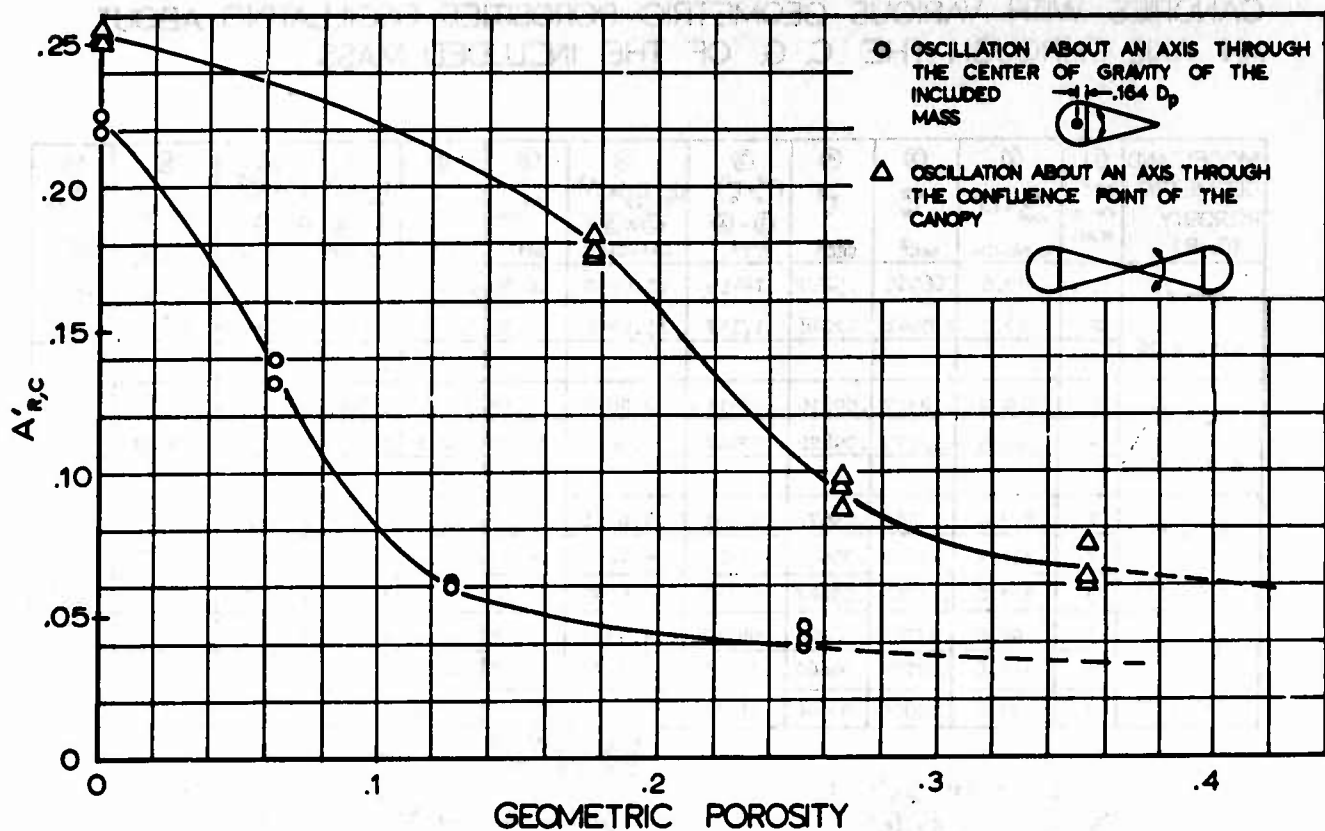


FIG 25. APPARENT MOMENT OF INERTIA COEFFICIENT ($A'_{R,C}$) vs GEOMETRIC POROSITY FOR RIBBON CANOPY MODELS OSCILLATING ABOUT TWO DIFFERENT AXES

18 per cent reduces the apparent moment of inertia in this case to about 70 per cent of its original value for zero porosity. At a geometric porosity of approximately 27 per cent, the apparent moment of inertia is reduced to nearly 37 per cent of its original value while at a geometric porosity of about 35 per cent, the moment of inertia drops to 26 per cent of its value for zero porosity.

The established influence of the porosity upon the dynamic inertia effects of the idealized parachute canopies coincides to a large extent with the findings of H. G. Heinrich (Ref 9), in which a significant reduction of the apparent mass with increasing parachute porosity was shown.

D. Concluding Remarks

In extending the experimental method of determining the apparent moment of inertia to account for geometric porosity effects, additional simplifying assumptions were involved. All viscous effects were ignored and potential irrotational flow was assumed. In view of the assumptions and idealizations involved, it is felt that the tests relating the apparent moment of inertia to geometric porosity should be viewed as of a general exploratory character rather than definite numerical validity. They help to indicate the relative magnitude of the change of apparent moment of inertia with geometric porosity.

REFERENCES

1. T. Von Karman. Note on Analysis of the Opening Shock of Parachutes at Various Attitudes.
2. H. Lamb. Hydrodynamics, 6th Edition, Dover Publications, 1945.
3. Milne-Thompson. Theoretical Hydrodynamics, 2nd Edition, 1949, MacMillan and Company, London.
4. A. F. Zahm. Flow and Force Equations for a Body Revolving in a Fluid, Parts IV and V, NACA TR 323, 1929.
5. M. P. Miller. An Accurate Method of Measuring the Moments of Inertia of Airplanes, NACA TN 351.
6. H. A. Soule and M. P. Miller. The Experimental Determination of the Moments of Inertia of Airplanes, NACA TR 467, 1933.
7. Yee Tak Yu. "Virtual Masses and Moments of Inertia of Discs and Cylinders in Various Liquids," Journal of Applied Physics, 1942, Vol 13, pp 66-69.
8. J. M. Stelson and F. T. Mavis. "Virtual Mass and Acceleration in Fluids," Trans., ASCE, Vol 22, pp 518-530, 1957.
9. H. G. Heinrich. "Experimental Parameters in Parachute Opening Shock Theory," Shock and Vibration Bulletin No. 19, Research and Development Board, Department of Defense, February, 1953, AD 9513.

Unclassified

Security Classification

DOCUMENT CONTROL DATA - R&D		
(Security classification of this report and abstract and indexing annotation must be entered when the overall report is classified)		
1. ORIGINATING ACTIVITY (City and State)		2a. REPORT SECURITY CLASSIFICATION
University of Minnesota Minneapolis, Minn.		Unclassified
		2b. GROUP
		n/a
3. REPORT TITLE		
Experimental Determination of the Apparent Moment of Inertia of Parachutes		
4. DESCRIPTIVE NOTES (Type of report and inclusive dates)		
Final Report April 1963 - May 1964		
5. AUTHOR(S) (Last name, first name, initial)		
Ibrahim, Shukry K.		
6. REPORT DATE	7a. TOTAL NO. OF PAGES	7b. NO. OF REFS
April 1965	43	9
8a. CONTRACT OR GRANT NO.	8a. ORIGINATOR'S REPORT NUMBER(S)	
AF33(657)-11184	FDL-TDR-64-153	
b. PROJECT NO. 6065		
c. 606503	8b. OTHER REPORT NO(S) (Any other numbers that may be assigned this report)	
d.	none	
10. AVAILABILITY/LIMITATION NOTICES		
Qualified users may obtain copies of this report from DDC. DDC release to CSFTI is not authorized. Foreign announcement and dissemination of this report is not authorized.		
11. SUPPLEMENTARY NOTES	12. SPONSORING MILITARY ACTIVITY	
none	AFFDL (FDFR) WPAFB, Ohio	
13. ABSTRACT		
<p>An experimental arrangement for determining the apparent moment of inertia of parachute canopy models is described. The rigid canopy models are attached to a simple torsion pendulum and the periods of oscillation of the models and suspension system in air and in water are measured and used to calculate the apparent moment of inertia of the model canopies. The validity of the experimental arrangement was verified by measuring the apparent mass of some simple geometric bodies such as spheres and cubes and comparing the results with known theoretical values. Models of the circular flat, ribbon and ribless guide surface canopy shapes were tested for angular motion about two different axes and the results are presented in nondimensional coefficient form.</p> <p>Additional results showing the effect of geometric porosity on the apparent moment of inertia of a ribbon type parachute canopy model are presented in the Appendix.</p>		

DD FORM 1473
1 JAN 64

Unclassified

Security Classification

14. KEY WORDS	LINK A		LINK B		LINK C	
	ROLE	WT	ROLE	WT	ROLE	WT
Apparent moment of inertia						
Parachute canopies						
Apparent mass						
Results from experiments						

INSTRUCTIONS

1. **ORIGINATING ACTIVITY:** Enter the name and address of the contractor, subcontractor, grantee, Department of Defense activity or other organization (*corporate author*) issuing the report.

2a. **REPORT SECURITY CLASSIFICATION:** Enter the overall security classification of the report. Indicate whether "Restricted Data" is included. Marking is to be in accordance with appropriate security regulations.

2b. **GROUP:** Automatic downgrading is specified in DoD Directive 5200.10 and Armed Forces Industrial Manual. Enter the group number. Also, when applicable, show that optional markings have been used for Group 3 and Group 4 as authorized.

3. **REPORT TITLE:** Enter the complete report title in all capital letters. Titles in all cases should be unclassified. If a meaningful title cannot be selected without classification, show title classification in all capitals in parenthesis immediately following the title.

4. **DESCRIPTIVE NOTES:** If appropriate, enter the type of report, e.g., interim, progress, summary, annual, or final. Give the inclusive dates when a specific reporting period is covered.

5. **AUTHOR(S):** Enter the name(s) of author(s) as shown on or in the report. Enter last name, first name, middle initial. If military, show rank and branch of service. The name of the principal author is an absolute minimum requirement.

6. **REPORT DATE:** Enter the date of the report as day, month, year, or month, year. If more than one date appears on the report, use date of publication.

7a. **TOTAL NUMBER OF PAGES:** The total page count should follow normal pagination procedures, i.e., enter the number of pages containing information.

7b. **NUMBER OF REFERENCES:** Enter the total number of references cited in the report.

8a. **CONTRACT OR GRANT NUMBER:** If appropriate, enter the applicable number of the contract or grant under which the report was written.

8b, 8c, & 8d. **PROJECT NUMBER:** Enter the appropriate military department identification, such as project number, subproject number, system numbers, task number, etc.

9a. **ORIGINATOR'S REPORT NUMBER(S):** Enter the official report number by which the document will be identified and controlled by the originating activity. This number must be unique to this report.

9b. **OTHER REPORT NUMBER(S):** If the report has been assigned any other report numbers (*either by the originator or by the sponsor*), also enter this number(s).

10. **AVAILABILITY/LIMITATION NOTICES:** Enter any limitations on further dissemination of the report, other than those

imposed by security classification, using standard statements such as:

- (1) "Qualified requesters may obtain copies of this report from DDC."
- (2) "Foreign announcement and dissemination of this report by DDC is not authorized."
- (3) "U. S. Government agencies may obtain copies of this report directly from DDC. Other qualified DDC users shall request through _____."
- (4) "U. S. military agencies may obtain copies of this report directly from DDC. Other qualified users shall request through _____."
- (5) "All distribution of this report is controlled. Qualified DDC users shall request through _____."

If the report has been furnished to the Office of Technical Services, Department of Commerce, for sale to the public, indicate this fact and enter the price, if known.

11. **SUPPLEMENTARY NOTES:** Use for additional explanatory notes.

12. **SPONSORING MILITARY ACTIVITY:** Enter the name of the departmental project office or laboratory sponsoring (*paying for*) the research and development. Include address.

13. **ABSTRACT:** Enter an abstract giving a brief and factual summary of the document indicative of the report, even though it may also appear elsewhere in the body of the technical report. If additional space is required, a continuation sheet shall be attached.

It is highly desirable that the abstract of classified reports be unclassified. Each paragraph of the abstract shall end with an indication of the military security classification of the information in the paragraph, represented as (TS), (S), (C), or (U).

There is no limitation on the length of the abstract. However, the suggested length is from 150 to 225 words.

14. **KEY WORDS:** Key words are technically meaningful terms or short phrases that characterize a report and may be used as index entries for cataloging the report. Key words must be selected so that no security classification is required. Identifiers, such as equipment model designation, trade name, military project code name, geographic location, may be used as key words but will be followed by an indication of technical context. The assignment of links, rules, and weights is optional.